AN ABSTRACT OF THE THESIS OF

Matthew S. Lewis for the degree of Master of Science in Microbiology presented on August 24, 2017

Title: The MAV_4644 dual-function channel protein with putative ADP-ribosyltransferase activity of *Mycobacterium avium* is required for virulence within host macrophages

Abstract approved: _____
Luiz E. Bermudez

Mycobacterium avium subspecies *hominissuis* (MAH) is an opportunistic pathogen that is ubiquitous in the environment and often isolated from faucets and showerheads. MAH mostly infects humans with an underlying disease, such as chronic pulmonary disorder (COPD), cystic fibrosis (CF), or are immunocompromised, though infections in patients without concurrent disease are increasing in prevalence. MAH is resistant to many antibiotics due to the impermeability of its envelope and the protection of its intracellular niche inside host macrophages, making the infections difficult to treat. Host macrophages produce nitric oxide and reactive oxygen intermediates to kill phagocytosed bacteria. However, MAH replicates in nitric oxide producing cells and is less virulent when inducible nitric oxide synthesis is suppressed in a murine host. To investigate the relationship between MAH and nitric oxide, an *in vitro* model was developed in murine macrophages. We show that MAH grows in macrophages stimulated with IFN-γ and producing nitric oxide. A transposon library screen of MAH for mutants incubated with nitric oxide donor indicated

that inactivation of the gene MAV_4644 (MAV_4644:Tn) resulted in nitric oxide susceptibility. Characterization of MAV_4644:Tn revealed that it is required for virulence in host macrophages. In silico analysis revealed MAV_4644 is a dual-function channel protein with putative ADP-ribosyltransferase activity. Protein binding assays indicate that MAV_4644 protein interacts with the host lysosomal peptidase, cathepsin Z. Cathepsins are key regulators of inflammation and antigen presentation within immune cells. Pathogenic mycobacteria have been shown to suppress the action of other cathepsins to establish their intracellular niche. Knock-down of cathepsin Z in host macrophages rescued the attenuated phenotype of MAV_4644:Tn. The data suggests cathepsin Z is involved in early mycobacterial killing within host macrophages and virulence factor MAV_4644 protein abrogates this process.

The MAV_4644 dual-function channel protein with putative ADP-ribosyltransferase activity of *Mycobacterium avium* is required for virulence within host macrophages

by
Matthew S. Lewis

A THESIS

Submitted to

Oregon State University

in partial fulfillment of
the requirements for the
degree of

Master of Science

Presented August 24, 2017
Commencement June 2018

Master of Science thesis of Matthew S. Lewis presented on August 24, 2017.

APPROVED:

Major Professor, representing Microbiology

Chair of the Department of Microbiology

Dean of the Graduate School

I understand that my thesis will become part of the permanent collection of Oregon State University libraries. My signature below authorizes release of my thesis to any reader upon request

Matthew S. Lewis, Author

ACKNOWLEDGEMENTS

Thank you to Luiz Bermudez for providing me the opportunity to complete my degree at Oregon State University and for his many contributions to my professional and personal development. Thank you also to my committee members, Brian Dolan and Dan Rockey for their support and advice. In addition, thanks to Sasha Rosa and Lia Danelishvili for lending their expertise on technical issues. Finally, I would like to thank my friends and family for their support and encouragement.

CONTRIBUTION OF AUTHORS

Drs. Luiz Bermudez, Lia Danelishvili and Sasha Rose contributed to experimental design and planning. Drs. Luiz Bermudez, Brian Dolan and Dan Rockey advised on manuscript revisions.

TABLE OF CONTENTS

LIST OF FIGURES

Figure Page

LIST OF FIGURES (continued)

LIST OF TABLES

CHAPTER 1. Introduction

Mycobacterium avium subspecies *hominissuis* (MAH) is a ubiquitous environmental saprophyte capable of infecting a broad host range of animals, including humans (Inderlied 1993). In addition to the zoonotic risks of transmission, MAH creates robust biofilms and is often isolated from outputs of modern chloraminated drinking water distribution systems, such as shower heads and faucets (Cook 2009, Gomez-Smith 2015). While MAH usually infects humans with an underlying lung disease, such as chronic obstructive pulmonary disorder (COPD), cystic fibrosis (CF), or are immunocompromised, MAH can cause progressive lung infections in patients without concurrent disease (Field 2004). The gut is also a route of entry for human infection with MAH, and both respiratory and gastrointestinal infections of MAH appear to be increasing in prevalence (Ishikane 2014, Lai 2010, Houqani 2011). Infection of MAH is difficult to treat and patients are typically given a combination therapy with two or three antimicrobial agents for one year due to the intrinsic resistance of MAH to many antibiotic drugs (Philley 2016). This intrinsic resistance can in part be attributed to the impermeability of the mycobacterial envelope, which is rich in hydrophobic mycolic acids (Marrakchi 2014). In addition, MAH reside and replicate within host macrophages, further isolating the bacterium from effective antibiotic treatment (Rocco 2011).

Overcoming the bactericidal properties of macrophages is key to the success of intracellular pathogens, such as mycobacteria (Amer 2002). One principal mode of circumventing macrophage killing by mycobacteria, is to arrest the maturation of the phagolysosome. Following phagocytosis, MAH resides in a non-acidified phagosome,

denoted the mycobacteria vacuole (MV) (Cook 2009). The MV fuses with early endosomes, is accessible to some endosomal proteins, restricts accumulation of proton-ATPases, halting acidification, and retains cathepsin D as an immature proenzyme (Sturgill-Koszycki 1996, Kelley 2003). To establish itself in its intracellular niche, MAH must first survive the oxidative burst produced by the NADPH oxidase complex during phagocytosis and engulfment by the host macrophage (Park 2003). Pathogenic mycobacteria produce at least two highly conserved superoxide dismutase enzymes (SODs), which are expressed at their surface or secreted, confer protection from oxidative stress and have been shown to be required for full virulence (Escuyer 1995, McNamara 2013, Liao 2013). NADPH oxidase complex has an important role in the early host response to bacterial infections, whereas the subsequent action of inducible nitric oxide synthase (NOS2) plays a more sustained role in controlling bacterial infections by adding nitric oxide to the milieu of toxic radicals in the MV (Fang 2004). The reactive oxygen species (ROS) and reactive nitrogen species (RNS) created by the interaction of chemical radicals in the phagosome, kill microbes by targeting protein thiols and metal centers, and blocking essential microbial physiological processes, such as respiration and DNA replication (Vazquez-Torres 2008, Bogdan 2015). Knock-out mice of either NADPH oxidase or NOS2 were more permissive to infection with intracellular pathogens such as *E. coli and S. typhimurium* (Shiloh 1999).

The role of NOS2 in pathogenic mycobacterial infections is intriguing because unexpectedly, NOS2 knockout mice, incapable of producing nitric oxide within their macrophage phagosomes, were more resistant to MAH infection than the wild-type mice controls (Gomes 1999, Orme 2014). Furthermore, nitric oxide production by MAH infected

macrophages was shown to inhibit phagocytosis of neighboring macrophages, possibly contributing to dissemination of MAH infection (Doi 1993). Conversely, pathogenic *Mycobacterium tuberculosis* H37Rv (MTB) is markedly more fit in NOS2 knock-out mice and restricts NOS2 assembly on the MV membrane in an *in vitro* macrophage model (Beisiegel 2009, Miller 2004). Understanding the role of nitric oxide in the survival and replication of pathogenic mycobacteria within host macrophages could identify virulence factors, required for intracellular growth, as future targets for antimicrobial therapy.

To this end, an *in vitro* model was developed to explore the ability of MAH to grow within nitric oxide producing macrophages. We show that the intracellular population of MAH increases in macrophages stimulated with IFN-γ and producing nitric oxide, while it decreases in unstimulated macrophages or cells with inhibited nitric oxide production. A transposon library was then screened to identify genes involved in this process. The MAH mutant carrying a transposon in gene MAV_4644 (MAV_4644:Tn) displayed markedly reduced virulence in the early stages of macrophage infection. MAV_4644 is putatively identified to encode an ADP ribosyltransferase and protein binding assays identified a potential interaction with the host lysosomal peptidase, cathepsin Z. This data suggests, cathepsin Z could be involved in early mycobacterial killing within macrophages and MAV_4644 protein serves to protect MAH from this action.

CHAPTER 1. Materials and Methods

Bacterial strains and culture: *Mycobacterium avium* subsp. *hominissuis* strain 104 (MAC104) was originally isolated from the blood of an AIDS patient and has been shown to

be virulent in mice infected by IV or respiratory routes. Mycobacteria were cultured on Middlebrook 7H10 agar supplemented with 10% oleic acid, albumin, dextrose and catalase (OADC) (Hardy Diagnostics) to log-phase at 37°C. Growth curves were conducted in Middlebrook 7H9 broth differentially supplemented with 10% OADC and glycerol. The optical density at 600nm was periodically measured with a spectrophotometer.

Cell Culture: Human monocyte THP-1 cell line (ATCC) was cultured in RPMI-1640 (Corning) supplemented with 10% fetal bovine serum (FBS, Gemini) at 37°C with 5% CO_2 as suspension cells. The cells were then counted with a hemocytometer, seeded at 80% confluency into 48-well plates and supplemented with 50 ng/ml of phorbol 12-myrisate 13-acetate (PMA, Sigma Aldrich) to differentiate the cells into adherent macrophages (Park 2006). After 24 hours, the culture media was replaced and the cells were allowed to rest another 24 hours before beginning experiments.

The murine macrophage-like RAW 264.7 cell line (ATCC) was cultured in DMEM (Corning) supplemented with 10% FBS at 37°C with 5% CO_2. For experiments, the RAW264.7 (ATCC TIB-71) murine macrophage-like cells were harvested by gentle washing with a serological pipette after being treated for 10 minutes at 37°C with 5mM EDTA in phosphate buffered saline (PBS). The murine macrophages were pelleted by centrifugation and resuspended in fresh culture media to remove the EDTA. Cells were counted with a hemocytometer and seeded such that 80% confluency was achieved at time of infection.

Invasion and survival assays: A single cell suspension of 3E8 colony forming units per ml (cfu/ml) of MAH was created in phosphate buffered saline (PBS) by visual comparison to a McFarland standard. The suspension was left still for 5 minutes to allow bacterial

aggregates to settle. The top half volume was removed for the infection inoculum. Host cells were inoculated at a multiplicity of infection of 10 in either 24-well or 48-well flat bottom plates and centrifuged for 10min at 800 rpm to synchronize the infections. Invasion and uptake were allowed to proceed for 1 to 2 hours at 37°C and 5% CO_2. Infected cells were then gently washed twice with HBSS and refreshed with the appropriate culture medium supplemented with 200 μg/ml gentamicin (Sigma) for 2 hours. The cells were then washed twice with HBSS (Corning). At this point the wells denoted time 0 were lysed by adding 0.1% Triton X-100 (VWR) for 10 minutes and disrupted with twenty pipette strokes, while the remaining wells were replenished with culture medium for collection at subsequent time-points. Cell lysates were serially diluted in PBS and plated onto Middlebrook 7H10 agar supplemented with 10% OADC (Hardy Diagnostics). Colonies were counted after 8-10 days incubation at 37°C.

To assess the effect of nitric oxide on MAH survival within RAW264.7 murine macrophages either 10 ng/ml of murine IFN-γ (Invitrogen) alone or 10 ng/ml of IFN-γ and 100 μM N-Monomethyl-L-arginine, monoacetate salt (L-NMMA, Cayman Chemical) (Kittel 2014) was added to the culture medium at time 0. Fully supplemented media was replenished at day 4. Uptake and survival was quantified as described above. Nitrite levels were assayed daily by collecting infection supernatants and performing the Greiss test following the manufacturer's protocol for the Greiss Reagent System (Promega).

MycoMarT7 transposon library creation and screen for nitric oxide susceptibility:

MycoMarT7 (Mmt7) is a phagemid with a kanamycin resistance gene under the control of T7 promoter (Sassetti 2001). MAC104 was transduced with MmT7 as previously described

(Rose 2016). A total of 930 MAH Mmt7 transposon mutant (Mmt7:Tn) individual colonies were each grown in 96-deep-well plates for 5 days in 300 μl of 7H9 broth supplemented with 10% OADC (Hardy Diagnostics) and 400 μg/ml kanamycin (Sigma) at 37°C with 210 rpm shaking. Two wells per plate were inoculated with MAC104 without kanamycin and one well was filled with media alone to serve as a blank. After 5 days of growth the cultures were mixed by gentle pipetting and 150 μl of bacteria were transferred to 96-well flat bottom plates and pelleted by centrifugation. The supernatant was removed and bacteria were carefully resuspended in 7H9 broth supplemented with 10% OADC, 400 ug/ml kanamycin and 100 μMol spermine NONOate, a nitric oxide donor (Calbiochem). The optical density was measured at 600nm in a plate-reading spectrophotometer (Biotek) and recorded as time 0. The plates were placed at 37°C with 210 rpm shaking for 3 hours, then moved to a 37°C incubator for an additional 2 days. The optical density was read at 600nm and the percent increase was determined. Mutants with increased susceptibility to nitric oxide were identified as those with 50% or less increased optical density when compared to wild type. Identified mutants were confirmed by repeating the screen.

Identification of Mmt7 transposon interrupted MAH genes: Mmt7 transposon insertion sites were identified via ligation-mediated PCR (LMPCR) as previously reported (Rose et al 2016). Briefly, genomic DNA was isolated, restriction digested, and ligated with custom adapters complementary to the cut sites. Products were then used as templates for the LMPCR reactions with primer sets designed to amplify a 150bp segment of the transposon and the region of interrupted gene at the insertion site. Amplicons were submitted to the

Center for Genome Research and Biocomputing at Oregon State University for Sanger sequencing.

***In silico* analysis and literature review of MAV_4644:** National Center for Biotechnology (NCBI) web server was utilized for conserved protein domain searches. The NCBI Basic Local Alignment Search Tool (BLAST) was utilized for nucleotide and protein alignment analysis (NCBI ref). A search for homologous proteins was performed on the Kyoto Encyclopedia of Genes and Genomes (KEGG) web server using the Sequence Similarity Database (SSDB) which ranks all possible pairwise protein alignments based on the Smith-Waterman similarity score and a dendogram was created based on the total scores (Sato 2001). The Constraint-Based Local Alignment Tool (COBALT) was utilized to visualize primary protein sequence alignments (Papadopolous 2007). Operon association of genes were investigated on the Database of Prokaryotic Operons (DOOR^2) web server (Mao 2009).

Expression of MAV_4644, MAV_4643, and MAV_4642 recombinant proteins and immunoprecipitation assays: The C-terminal domain of MAV_4644, 2100bp and 2178bp, corresponding to the VIP2 ADP-ribosyltransferase domain, denoted MAV_4644_CTD, as well as MAV_4643 and MAV_4642 were cloned into the pET6xHN-C vector (Clontech) using standard c methods (Sambrooks). The recombinant protein products were expressed in BL21 (DE3) competent *E. coli* (Invitrogen) and purified with the His-60 Ni Superflow Gravity Column Purification Kit (Takara) following the manufacturer's recommendations. The expression and purification of the recombinant proteins were confirmed by SDS_PAGE and Western blot using an anti-6xHN antibody (Takara).

For the immunoprecipitation assay, protein purification was arrested before elution and

cleared host cell lysate was added to the columns, which were then incubated at 4°C for 24 hours with gentle inversion. After allowing the beads to settle, the columns were drained and washed with 5 ml of equilibration buffer followed by 5 ml of wash buffer before being eluted into 1 ml fractions with elution buffer. The concentration of protein in each fraction was assessed by SDS-PAGE and Coomassie staining. The second fraction contained the majority of the protein in every pull-down. These fractions were each concentrated to 50 µl using a Nanosep 3K centrifugal filter device (VWR). The samples were prepared with SDS and PAGE was performed until the samples were focused and passed approximately 1cm through the gel. A one square cm section of gel was then carefully excised per sample and purified using the Protease MAX in-gel trypsin digestion kit (Promega). A lysate of un-induced *E. coli* DE3 was used as a negative control in place of the recombinant MAH proteins. Protein samples were sequenced at the Oregon State University Mass Spectrometry Center following their standard protocols. Proteome Discoverer v 1.3.0, Mascot v 2.3 and Scaffold were used for data analysis. The Uniprot *Homo sapien* database was used to identify host proteins. The proteins identified in the negative sample were subtracted and the CRAPome database was used to filter out nonspecific interactions. (Mellacheruvu et al, 2013). All immunoprecipitation experiments were performed in tandem.

Far Western Blotting: THP-1 cells were seeded at 80% confluency in a T-75 flask (Corningware) and differentiated with 50 ng/µl of PMA. After 24 hours in 37°C with 5% CO_2, the cells were washed with PBS and fresh RPMI-1640(Corning) with 10% FBS (Gemini) and allowed to rest for an additional 24hours. The cells were washed twice with PBS and 2 ml of

CellLytic M (Sigma) supplemented with 10 µl Protease inhibitor for Mammalian Cells (Sigma) was then added. The flask was agitated at room temperature for 15 minutes to allow for lysis. The lysate was aliquoted, 1ml each, to two clean Eppendorf tubes and spun at 10,000XG for 20 minutes in a table-top centrifuge. The protein concentration of the clarified lysate was determined by reading the optical density at 260nm with a Nanodrop spectrophotometer. Three separate 50 µg samples of clarified lysate were resolved with SDS-PAGE, transferred to a nitrocellulose membrane and probed individually with either MAV_4644_CTD, cathepsin Z antibody (Thermo), or 6XHN antibody (Takara). The membranes were then probed with the appropriate IRDye fluorescent antibody (Li-Cor) and visualized with a Li-cor imaging system.

Knock-down of Cathepsin Z and infection with MAH and MAV_4644:Tn: THP-1 cells were seeded to 60% confluency in 48-well plates and differentiated with 20 ng/ml PMA in RPMI-1640 (Corning) supplemented with 10% FBS (Gemini) for 24 hours, at which point the medium was refreshed. After allowing the cells to rest for 24 hours the medium was refreshed again just before adding the freshly prepared transfection complex. The transfection complex was prepared with either cathepsin Z interfering RNA (DsiRNA hs.Ri.CTSZ.13.2, IDT) or non-targeting interfering RNA (DsiRNA, IDT) and Viromer Green transfection reagent (Lipocalyx) following the manufacturer's protocol with the following specifications. The working volume per well was 500 ul and each transfection complex was made at 100 nM siRNA in 50 µl Viromer Green buffer. Uptake of transfection complex was verified with the TYE 563 Transfection Control (IDT). The transfection medium was replaced at 24 hours with RPMI-1640 supplemented with 10% FBS (Gemini) and refreshed in 24 hour

intervals for 3 days. Cells were then infected with MAC104 and MAV_4644:Tn. After selected time intervals, cells were lysed to assay bacterial survival and to assess cathepsin Z protein levels. The cell lysates were resolved with SDS-PAGE, transferred to a nitrocellulose membrane, probed with cathepsin Z (Thermo) and B-actin (Abcam) antibodies, and visualized with a LI-COR imaging system.

Statistical Analysis: Experiments in this research were repeated at least 2 times. Data is displayed as means of replicates ± standard error. The Student's t-test was used to compare experimental and control groups. Differences were considered significant when $p < 0.05$. Graph Pad Prism version 5.0 software was used for statistical analysis.

CHAPTER 1. Results

MAH replicates within IFN-γ macrophages that produce nitric oxide

To investigate the role of host cell nitric oxide production on the intracellular survival of MAH, a long term *in vitro* infection model utilizing the RAW264.7 murine macrophage cell line was developed. The cells were differentially treated with interferon-gamma, and the well-established nitric oxide synthase inhibitor, N-monomethyl-L-arginine, monoacetate salt (L-NMMA) (Kittel 2014). The infections were carried out for seven days with daily nitrite levels measured by the Griess assay. Nitrite is a stable decomposition product of nitric oxide and is often measured to ascertain nitric oxide production in cells and tissues (Campos-neto 1998). MAH was taken-up by cultured macrophages at ~15% of the inoculum in all treatment groups (data not shown). The only treatment group permissive to MAH growth was the interferon-gamma activated group, in which the MAH intracellular population

increased ~3-fold by day 7 **(figure 1a).** The corresponding nitrite levels inform that, while interferon-gamma treated cells produce higher levels of nitric oxide, infection with MAH alone is enough to trigger significant production of nitric oxide **(figure 1b).** The group treated with l-NMMA produced markedly less nitric oxide and was the least permissive group to MAH, though the number of recovered intracellular MAH was not statistically different than the untreated group. The data indicate that RAW264.7 macrophages are permissive to MAH replication when treated with IFN-γ and producing endogenous levels of nitric oxide.

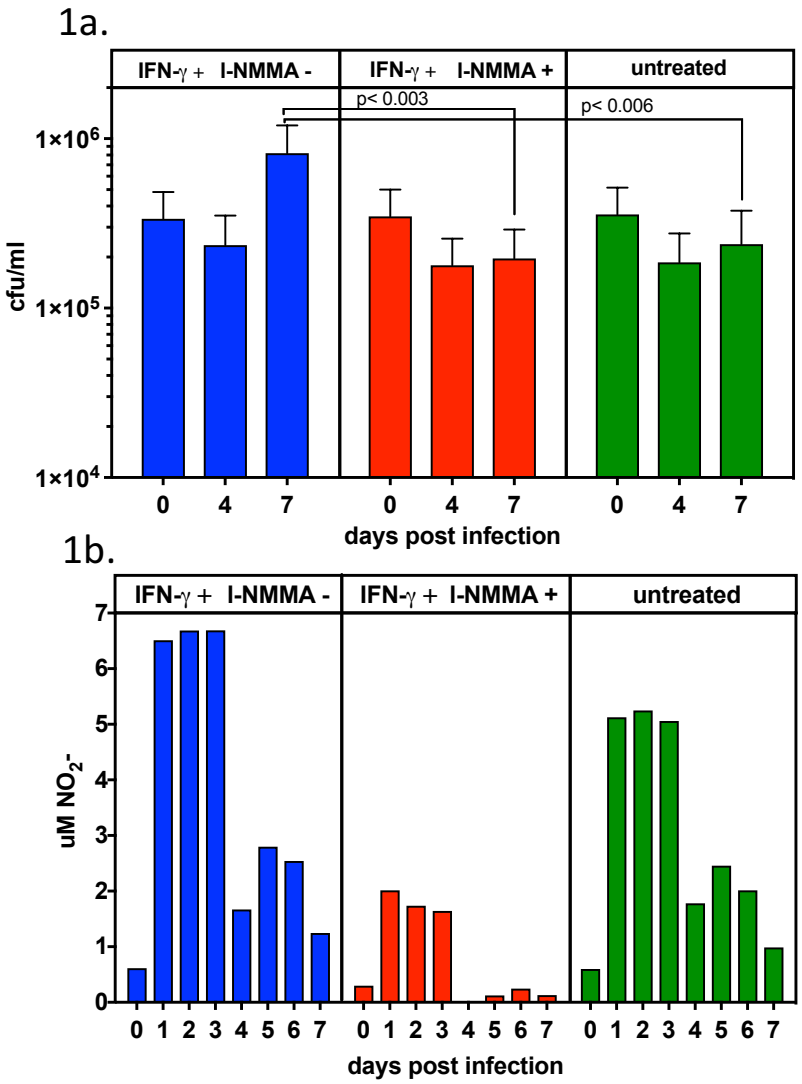

Figure 1: **a**. RAW264.7 murine macrophages were cultured in DMEM supplemented with 10%FBS in 24-well plates and infected with MAC104 for 2 hours at 37°C and 5% CO_2. The cells were washed twice with HBSS and incubated for an additional 2 hours in DMEM supplemented with 10%FBS and 200ug/ml amikacin. The cells were washed twice more with HBSS and culture media was replaced, differentially treated with IFN-γ and L-NMMA. At reported time points, the cells were lysed with 0.1% Triton X-100, serially diluted, plated on 7H10 agar and incubated at 37°C for 8-10 days before colonies were counted to assay cfu/ml. Data is the average of three separate trials. The Student's *t*-test was used to determine p-values as reported. **b.** The nitrite levels were assayed daily by collecting infection supernatants and performing the Greiss test. Data is representative of three separate trials.

Nitric oxide susceptibility of MAH

The minimum inhibitory concentration (MIC) of spermine NONOate, a chemical nitric oxide donor, was determined to be higher than 5 mM for MAH (data not shown). Due to the high MIC of this compound the minimum bacteriostatic concentration (MBC) of spermine NONOate on MAH was determined. It was shown that between 250 μM and 5000 μM spermine NONOate similarly inhibited the growth of MAH for 48 hours and a dose response effect of growth inhibition was observed from 0 to 100 μM **(figure 2).** It was determined that 100 μM of spermine NONOate was near the threshold of sensitivity for inhibiting wild-type growth, thus this concentration was used in the transposon screen to isolate nitric oxide sensitive mutants.

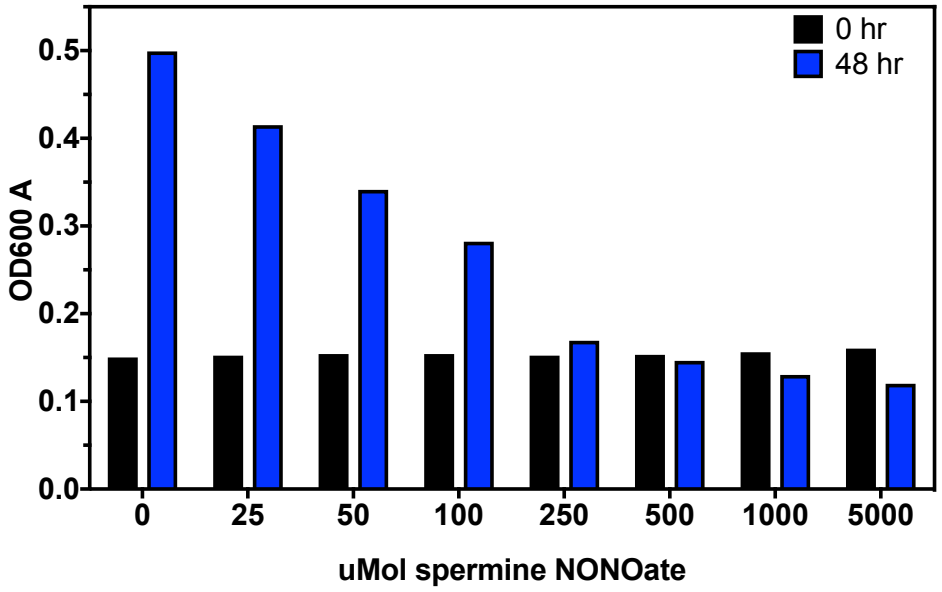

Figure 2: *In vitro* susceptibility of MAC104 to spermine NONOate. MAC104 was grown to OD_{600} of 0.15 in 7H9 broth supplemented with 10% OADC in a 37°C shaker. Spermine NONOate, a nitric oxide donor, was added at reported amounts and the cultures were incubated for an additional 48 hours. The data is representative of three separate trials.

Isolation of MAH Mmt7 transposon mutants susceptible to low bacteriostatic concentrations of nitric oxide

To identify the molecular mechanisms of nitric oxide resistance and possibly the effect of nitric oxide on intracellular growth in MAH, a mycobacteriophage-based transposon library was created in MAC104 and 930 individual transposon mutants were screened for susceptibility to a sub-bactericidal level of nitric oxide. A total of 46 mutants displayed increased susceptibility, and the transposon insertion site was determined to be located within a putative coding sequence in 34 of the susceptible mutants **(table 1).** Gene ontology analysis of the identified coding sequences revealed that 24% were involved in catalytic activity, 18% in metabolism, 13% in oxidoreductase activity and 7% were involved in membrane structure or synthesis **(figure 3)** (Ashburner 2000).

Gene ID	Clone	% of WT	Description	Uniprot Accession	Locus tag
MAV_0118	2B2	16.2	Ppe family protein	A0A0H2ZRQ5	MAV_RS00580
MAV_0158	1D3	40.1	Subtilase family protein	A0A0H2ZRQ5	MAV_RS00770
MAV_0175	2D10	33.2	monooxygenase, flavin-binding family protein	A0A0H2ZWF6	MAV_RS00840
MAV_0249	2F1	33.7	Uncharacterized protein	A0A0H2ZY15	MAV_RS01200
MAV_0273	1A9	39.7	Uncharacterized protein	A0A0H2ZWS7	MAV_RS01315
MAV_1264	1 E10	2.3	Short chain dehydrogenase/reductase family protein	A0A0H2ZTF8	MAV_RS06065
MAV_1621	1G5	42.0	Uncharacterized protein	A0A0H2ZZA4	MAV_RS07760
MAV_1812	2F10	31.9	3-hydroxyacyl-CoA dehydrogenase type-2	A0A0H3A4S5	MAV_RS08680
MAV_1816	1 E8	13.2	Uncharacterized protein	A0A0H2ZUN3	MAV_RS08700
MAV_2256	2D12	25.1	Gp108 protein	A0A0H3A3J1	MAV_RS10765
MAV_2426	1B12	-1.5	RNA polymerase sigma factor	A0A0H2ZZS1	MAV_RS11565
MAV_2564	1F10	-6.8	Aldehyde dehydrogenase (NAD) family protein	A0A0H2ZWS2	MAV_RS12255
MAV_2590	2H4	33.9	Putative acyl-CoA dehydrogenase	A0A0H3A2H6	MAV_RS12365
MAV_2591	1H11	-6.5	Amidohydrolase 2	A0A0H2ZVD5	MAV_RS12360
MAV_2686	1B4	43.9	Uncharacterized protein	A0A0H2ZUN8	MAV_RS12825
MAV_2767	1 E3	40.1	Acyl-CoA dehydrogenase, C-domain protein	A0A0H3A0C8	MAV_RS13195
MAV_3056	1B6	39.4	Linear gramicidin synthetase subunit D	A0A0H2ZTY5	MAV_RS14575
MAV_3210	1H4	34.8	Glycogen debranching enzyme GlgX	A0A0H2ZZU9	MAV_RS19660
MAV_3286	2F7	36.0	Uncharacterized protein	A0A0H2ZX00	MAV_RS15695
MAV_3296	2F3	43.5	Uncharacterized protein	A0A0H2ZRF2	MAV_RS15740
MAV_3337	1F1	11.1	Monooxygenase	A0A0H2ZWN3	MAV_RS15945
MAV_3464	2F6	29.9	GTP pyrophosphokinase	A0A0H3A3N2	MAV_RS16570
MAV_3808	2 E11	38.2	2'-hydroxybiphenyl-2-sulfinate desulfinase	A0A0H3A3M7	MAV_RS18245
MAV_4014	2A4	39.1	Ppe family protein	A0A0H2ZTW6	MAV_RS19230
MAV_4124	2F12	27.4	Dehydrogenase	A0A0H2ZX25	MAV_RS19785
MAV_4249	2D11	41.6	3-ketosteroid dehydrogenase	A0A0H3A167	MAV_RS20390
MAV_4313	1 E12	0.9	Isocitrate dehydrogenase, NADP-dependent	A0A0H2ZT90	MAV_RS20695
MAV_4573	1G2	34.6	Putative methyl transferase	A0QLB4	MAV_RS21960
MAV_4644	1F2	29.0	Putative NAD(+)--arginine ADP-ribosyltransferase	A0QLI5	MAV_RS22305
MAV_4647	2G2	38.2	Cyclopropane-fatty-acyl-phospholipid synthase 2	A0A0H2ZZ17	MAV_RS22320
MAV_4791	1D5	34.1	Dehydrogenase	A0A0H2ZUD0	MAV_RS23020
MAV_4916	1A11	22.1	Short chain dehydrogenase/reductase family protein	A0A0H3A2P2	MAV_RS23625
MAV_5140	1D2	40.9	NAD(P) transhydrogenase beta subunit	A0A0H2ZXD2	MAV_RS24655
MAV_5205	2F8	38.4	Short chain dehydrogenase/reductase family protein	A0A0H3A044	MAV_RS24970

Table 1: Nitric oxide susceptible MAH mutant Mmt7 transposon interrupted gene list. Mutants were identified as those with 50% or less increased optical density when compared to wild type after 48 hours of growth in 7H9 broth supplemented with 10% OADC and 100 μM spermine NONOate. MmT7 transposon insertion sites were identified by LM-PCR and Sanger sequencing.

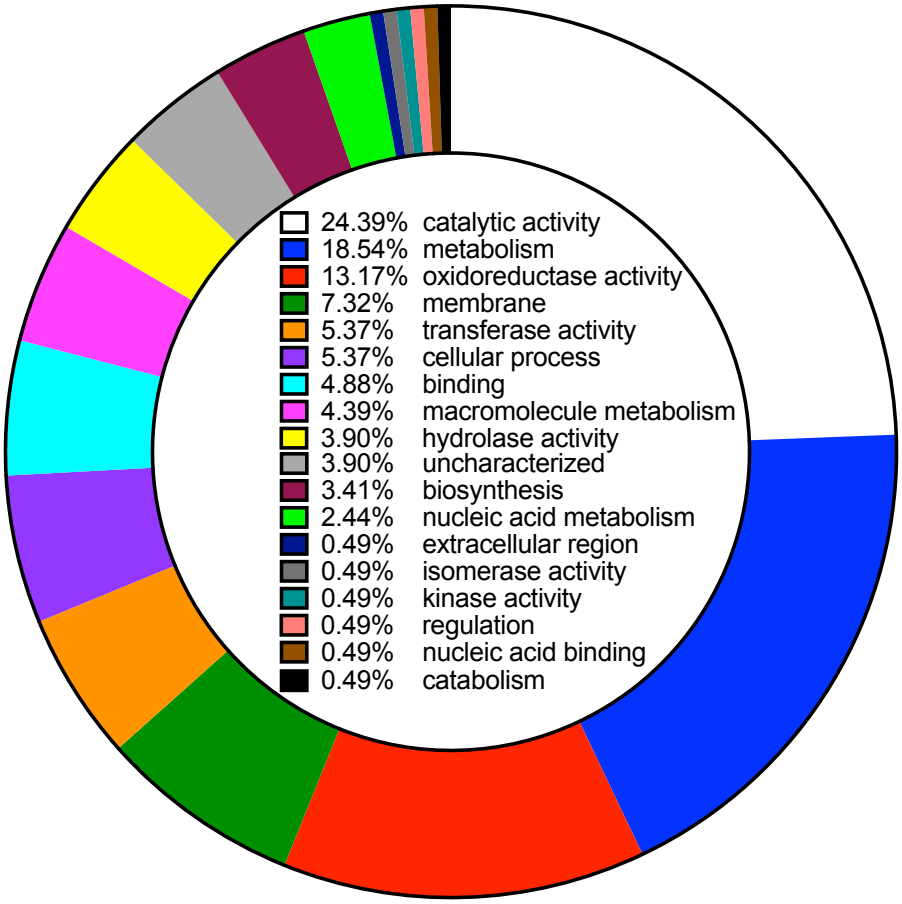

Figure 3: Gene Ontology analysis of MAH Mmt7 transposon mutants identified in spermine NONOate susceptibility screen. The CateGOrizer web server was used to batch analyze the Gene Ontology classification categories (https://www.animalgenome.org/tools/catego/).

Intracellular survival of MAH Mmt7 Tn mutants within macrophages

To determine whether the MAH Mmt7 Tn mutants identified in the transposon library screen displayed aberrant infection kinetics when compared to wild-type MAH, the 34 successfully sequenced mutants were individually subjected to the long-term infection model described above. It was determined that susceptibility to nitric oxide is not related to intracellular growth in this group of mutants as 32 of the 34 mutants displayed infection kinetics comparable to that of wild-type MAH **(figure 4).** The MAH mutant carrying a transposon within MAV_4644 (MAV_4644:Tn) was attenuated in RAW264.7 macrophages

displaying nearly a log loss in cfu/ml at 7 days, whereas the MAH mutant carrying a transposon within MAV_4014 (MAV_4014:Tn) displayed increased growth, consistently growing a 2 to 3 fold larger intracellular population than wild type MAH regardless of the inhibition of nitric oxide **(figure 5a).** The uptake percentage, which could be considered survival at 4 hours post infection was significantly divergent between the three strains. MAC104 was taken up at ~12%, while MAV_4644:Tn was taken up ~9%, and MAV_4014:Tn at ~20% **(figure 5b).**

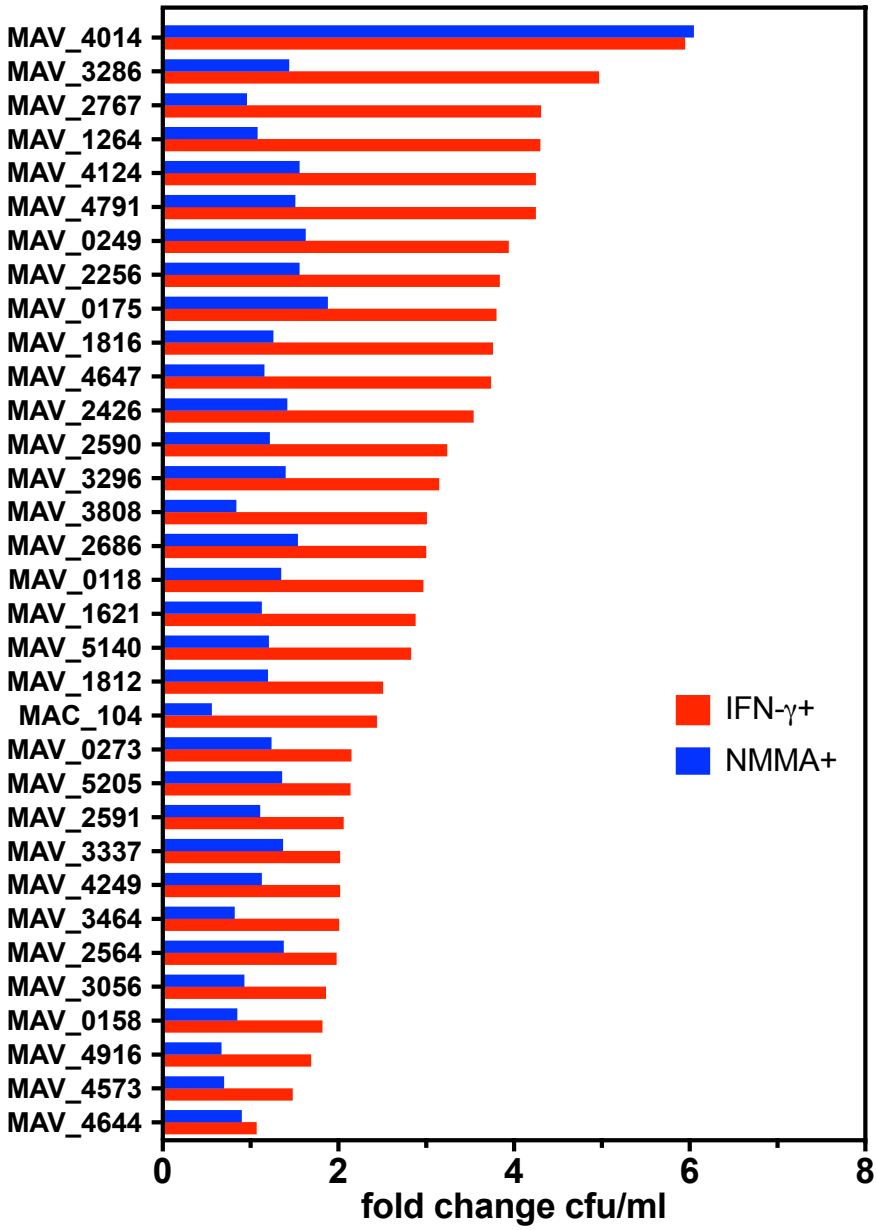

Figure 4: RAW264.7 murine macrophages were cultured in DMEM supplemented with 10%FBS in 24-well plates and infected separately with MAC104 and Mmt7:Tn for 2 hours at 37°C and 5% CO_2. The cells were washed twice with HBSS and incubated for an additional 2 hours in DMEM supplemented with 10%FBS and 200ug/ml gentamicin. The cells were washed twice more with HBSS and culture media was replaced, differentially treated with IFN-γ and L-NMMA. At day 3 the media was refreshed and at day 6 the cells were lysed with 0.1% Triton X-100, serially diluted, plated on 7H10 agar and incubated at 37°C for 8-10 days before colonies were counted to assay cfu/ml. Fold change was calculated by dividing day 6 cfu/ml by day 0 cfu/ml.

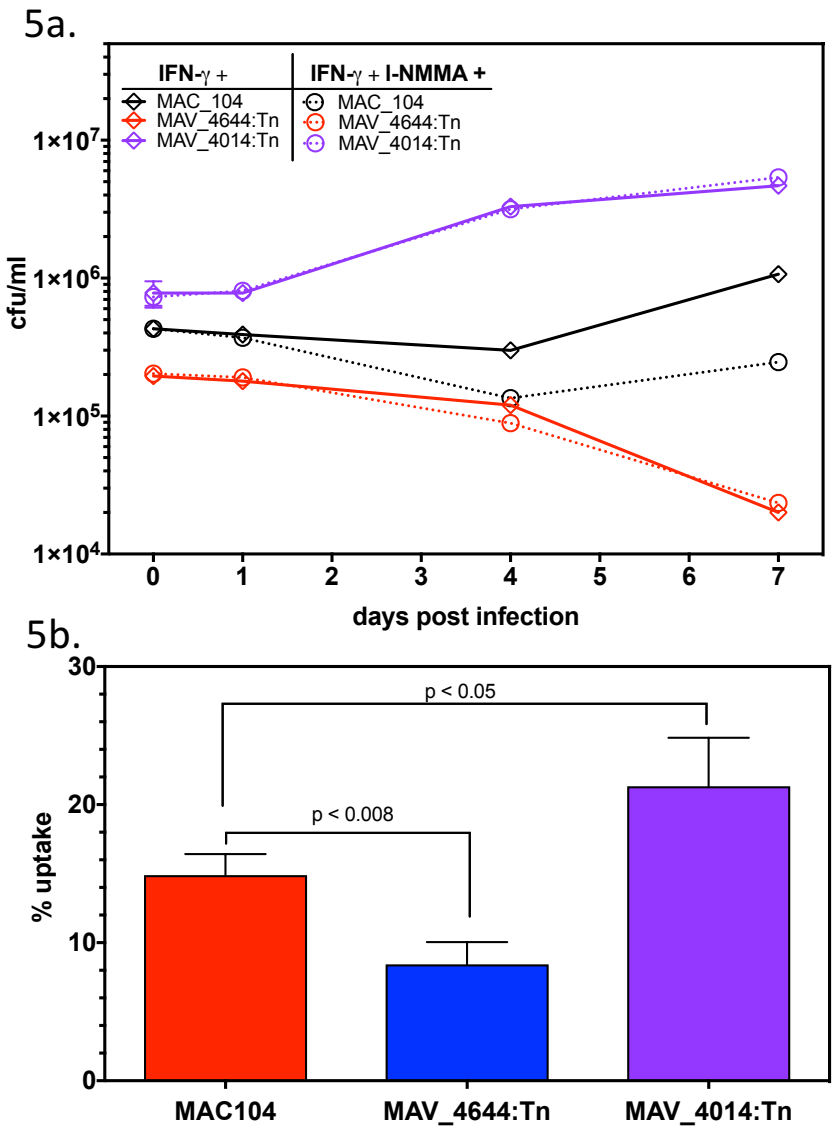

Figure 5: a. RAW264.7 murine macrophages were cultured in DMEM supplemented with 10%FBS in 24-well plates and infected separately with MAC104, MAV_4644:Tn, and MAV_4014:Tn for 2 hours at 37°C and 5% CO_2. The cells were washed twice with HBSS and incubated for an additional 2 hours in DMEM supplemented with 10%FBS and 200µg/ml gentamicin. The cells were washed twice more with HBSS and culture media was replaced, differentially treated with IFN-γ and L-NMMA. At reported time points, the cells were lysed with 0.1% Triton X-100, serially diluted, plated on 7H10 agar and incubated at 37°C for 8-10 days before colonies were counted to assay cfu/ml. The Student's *t*-test was used to determine p-values as reported. **b**. Percent uptake of MAC104, MAV_4644:Tn, MAV_4014:Tn was calculated by dividing the cfu/ml at time 0 by the initial inoculum cfu/ml and multiplying by 100. The Student's *t*-test was used to determine p-values as reported.

***In silico* analysis of MAV_4644**

The MAH gene MAV_4644 is predicted to encode an 825 amino acid ADP-ribosyltransferase (NCBI Ref.Seq. WP_011726171.1). The interval of amino acid 675 to 822 corresponds to VIP2, a protein family of actin-ADP-ribosylating toxins **(table 2).** GC content of the segment of the gene encoding this region of the protein is 52%, while the GC content for the remainder of the gene is 73%, indicating possible horizontal gene transfer. The C-terminus of the protein from amino acid 7 through 92 contains a WXG100 motif, a membrane translocation signal for type VII secretion systems (Bitter et al 2009). Also identified is a largely disordered region from amino acid 455 to amino acid 655, which aligns to 4 different domains each with a different function **(table 2).** In addition, this region is very rich in proline, accounting for about 31% of the total residues, while the other regions of the protein are approximately 5% proline.

Name	Accession	Description	Interval	E-value
WXG100	pfam06013	Proteins of 100 residues with WXG	7-92	0.00371
DedD	COG3147	Cell division protein DedD	455-527	0.00631
PHA03247	PHA03247	Large tegument protein UL36	455-655	5.69E-09
Atrophin-1	pfam03154	Atrophin-1 family	459-634	2.74E-06
rad23	TIGR00601	UV excision repair protein Rad23	475-543	0.00525
ADPrib_exo_Tox	pfam03496	ADP-ribosyltransferase exoenzyme	675-822	4.03E-15
VIP2	cd00233	VIP2; A family of actin-ADP-ribosylating toxin	675-820	1.18E-14

Table 2: Conserved domain analysis of MAV_4644 protein

To further investigate the potential function of MAV_4644 protein a similiarity search was performed on the Kyoto Encyclopedia of Genes and Genomes (KEGG) using the Sequence Similarity Database (SSDB) which ranks all possible pairwise protein alignments based on the Smith-Waterman similarity score (Sato et al, 2001). The top ranked homologs

are also annotated as putative ADP-ribosyltransferases and most of the remainder are annotated as either conserved hypothetical proteins or putative alanine and proline rich proteins. The top homologs were hierarchically arranged into a taxonomical dendogram based on similarity scores of each proteins' pairwise alignment with MAV_4644 protein and reported by species **(figure 6).**

One homolog, the *M. tuberculosis* protein Rv3903c has recently been well characterized as a channel protein with necrosis-inducing toxin function (CpnT) (Danilchanka 2014). The N-terminal domain of CpnT (NTD: amino acid 1-443) is an outer membrane channel protein required for uptake of glycerol. The C-terminal domain (amino acid 720-846) is released from the cell surface by proteolytic cleavage (Danilchanka et al, 2014). The released toxin, denoted TNT hydrolyzes NAD+, completely depleting this essential coenzyme and leading to necrotic cell death of the infected host cell (Sun 2015).

A primary sequence alignment performed on COBALT (Papadopolous 2007) between MAV_4644 protein and CpnT reveals a greatly conserved N-terminus with high identity and no gaps in the alignment until amino acid 441 of MAV_4644 protein **(figure 7).** A protein BLAST (pBLAST) alignment on the National Center for Biotechnology (NCBI) web server of the N-terminal domains between amino acid 1 and 435 of both proteins yields 100% query coverage with an E-value of 1E-166. A pBLAST alignment of the whole proteins as well as the disordered region also shows considerable conservation through amino acid 546. However, the C-terminal regions of both proteins have significantly divergent primary sequences, as pBLAST was only able to align 10% of these domains.

MAV_4644 was predicted to reside in a three gene operon with MAV_4642 and

MAV_4643 (Mao et al, 2009 and Dam et al, 2007). MAV_4642 protein (GenBank: ABK64648.1) and MAV_4643 protein (GenBank: ABK68102.1) are both annotated as conserved hypothetical secretion proteins as they both contain the WXG100 motif, typical of type VII secretion targets (Bitter et al 2009). A similarity search on KEGG quickly identified homologs to MAV_4642 and MAV_4643, as the ESAT-6 like proteins esxF and esxE respectively. The alignments performed using pBLAST between MAV_4642, MAV_4643 and their respective homologs esxf and esxE of *M. tuberculosis* strain H37Rv displayed conservation of the primary sequences. A comparison of the complete operons between the two strains reveals syntenic conservation of gene order, though the immunizing factor encoded by Rv3904 is lacking in MAH **(figure 8)** (Sun et al, 2015).

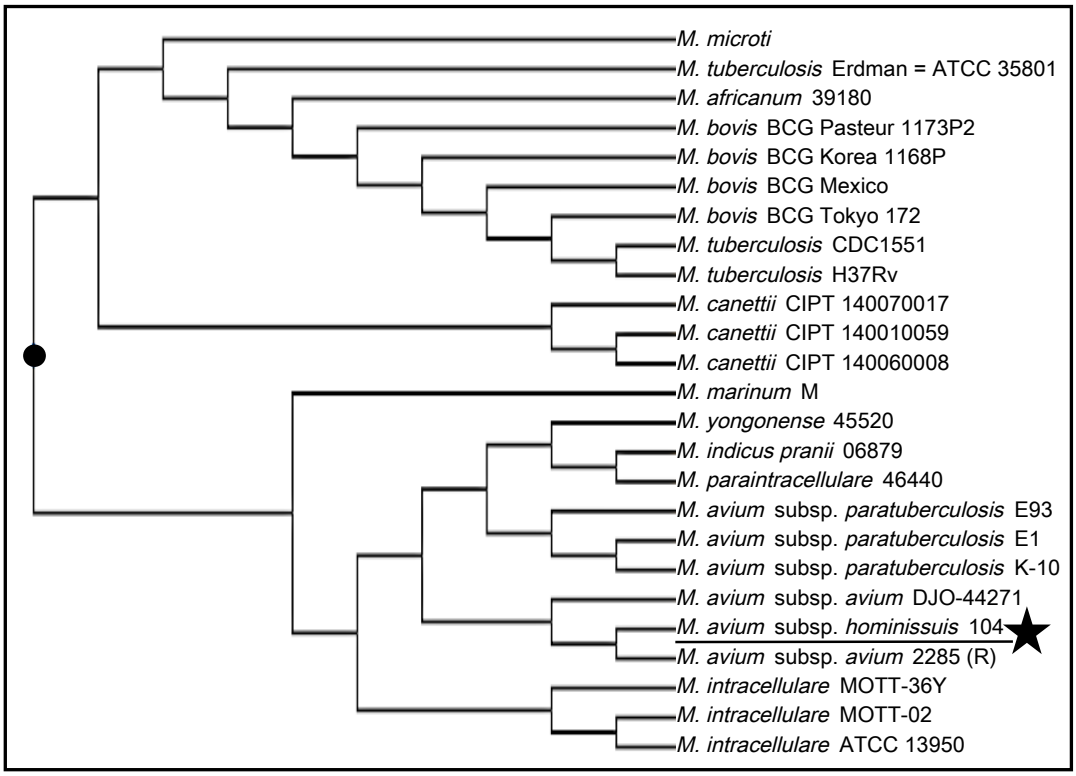

Figure 6: Dendogram of MAV_4644 protein homologs displayed by species. Proteins were clustered by relative pairwise homology to the primary protein sequence of MAV_4644

(underlined and starred), and ranked, based on the Smith-Waterman similarity score totals of pairwise alignments. The Kyoto Encyclopedia of Genes and Genomes was utilized to assemble the dendogram.

```
1    MAPLACDPTALDHAGATVVAAGESLGSVISTLTAALAGTSGMAGDDPVGAALGRRYDGAAAKLIQAMADTRNGLCSIGDG  80
1    MAPLAVDPAALDSAGGAVVAAGAGLGAVISSLTAALAGCAGMAGDDPAGAVFGRSYDGSAAALVQAMSVARNGLCNLGDG  80

81   VRMSAHNYAVAEAMSDLAGRASALPAPQVTGPLTVGAPPSAVGHGSGAPAGWGWVAPSIGMIWPTGDSAKLRAAAAAWAT  160
81   VRMSAHNYSLAEAMSDVAGRAAPLPAPPPSGCVGVGAPPSAVGGGGGAPKGWGWVAPYIGMIWPNGDSTKLRAAAVAWRS  160

161  AGANFMAAETAAGGGTMAAIGAQQIPEGAAINKALADASSATADVARQCQTIAAQLNSYAAKVDQVHAAILDLLSRICDP  240
161  AGTQFALTEIQSTAGPMGVIRAQQLPEAGLIESAFADAYASTTAVVGQCHQLAAQLDAYAARIDAVHAAVLDLLARICDP  240

241  LTGIKEVWDLLTDEDEDEIKKIADDIRTVVDNFGREADTLGGQIEATVSAVAAATENMSHWAGKEWDHFLHGTPVGRALN  320
241  LTGIKEVWEFLTDQDEDEIQRIAHDIAVVVDQFSGEVDALAAEITAVVSHAEAVITAMADHAGKQWDRFLHSNPVGVVID  320

321  QVGQAFKGVGEEGWGFLKGLYEVSPNRMLLDPVGYGKTMAGMVEGAGTLVGLGPDGVPGAFDAWKALGKDVTHWDEWGSN  400
321  GTGQQLKGFGEEAFGMAKDSWDLGPLRASIDPFGWYRSWEEMLTGMAPLAGLGGENAPGVVESWKQFGKSLIHWDEWTTN  400

401  PAEALGKSTFDVATLALPGGPLSKLGKFGHSAADALKGLKK---PPGVPKPPEVKPPAAPKAPDSGQPAPSGKPGPVAPS  477
401  PNEALGKTVFDAATLALPGGPLSKLGSKGRDILAGVRGLKERLEPTTPHLEPPATPPRPGPQPPRIEPPESGHPAP-APA  479

478  GKPAPGPADGPLPHSPTESKPPAGGTPPAAEPPKPTAAPHSGEPKPIATPPESVGKPVTPAPAEGAPAQPHEPVSARVPP  557
480  AKPAPVPANGPLPHSPTESKPPPVDRP--AEPVAPSSASAGQPRVSAATTPGTHVPHGLPQPGEHVPAQAP-------PA  550

558  TVPAADTPAPSAPAASMSAASGPPMPPTPSLPEPASLPSGPSGDLPAETPPTAGIPHSGEPSAPSSVPPHFPDTPTHGLG  637
551  TTLLGGPPVESAPATAHQ----PQWATTPAAPAAAPHST------PGGVHSTESGPHGRSLSAHGSEPTH--DGASHGSG  618

638  DGGAHGPPESDPKNANGHGPH----------------------DASLDSGSDHHLPLHPLDSDDLAALAHYTGPGYQELNF  696
619  HGSGSEPP-------GLHAPHREQQLAMHSNEPAGEGWHRLSDEAVDPQYGEPLSRHWDFTDNPADRSRINPVVAQLMED  691

697  ALREGALDVSQQA----------RVDALQKALEKLPVYEGAVVRGTNLPADVLEQYRPGEVITEAAFTSTSTDHTVAQS  765
692  PNAPFGRDPQGQPYTQERYQERFNSVGPWGQQYSNFPPNNGAV------PGTRIAYTNLEKFLSDYGPQLDRIGGDQGKY  765

766  SAFAGNTEFRIWSTTGRDVSSVSMYPDEKEILFPAGSKFYVVSKTVDPQTG----------------RTIIEMIER---  825
766  LAIMEHGRPASWEQRALHVTSLRDPYHAYTIDWLPEGWFIEVSE-VAPGCGQPGGSIQVRIFDHQNEMRKVEELIRRGVL  844

     --
845  RQ  846
```

Figure 7: A primary sequence alignment performed on COBALT between MAV_4644 protein of MAH and CpnT of MTB H37Rv. Matches are marked in red, mismatches in blue, and gaps in grey.

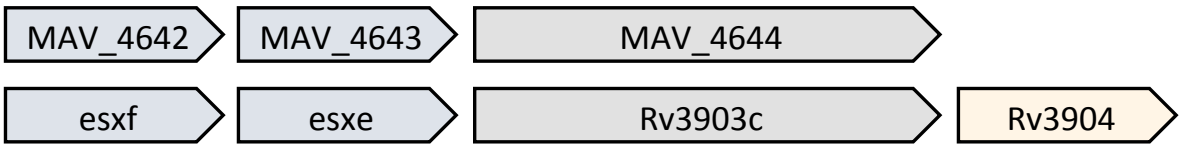

Figure 8: Schematic representation of the syntenic conservation of the MAV_4644 operon of MAH and the Cpnt operon of MTB.

Characterization of MAV_4644:Tn

To determine if the observed attenuation of MAV_4644:Tn in murine macrophages can be attributed to differences in growth rate, growth curves were ran in rich media. MAV_4644:Tn displayed the same growth kinetics as MAC104 in 7H9 broth supplemented with 10% OADC **(figure 9)**. Furthermore, to investigate if MAV_4644 protein is required for MAH growth on glycerol, such as CpnT is in *M. tuberculosis* H37Rv, 7H9 broth was prepared without OADC, which removes the dextrose and leaves only glycerol as an energy and carbon source. The comparative growth curves ran in this media revealed that MAV_4644 is not required for uptake of glycerol **(figure 9).**

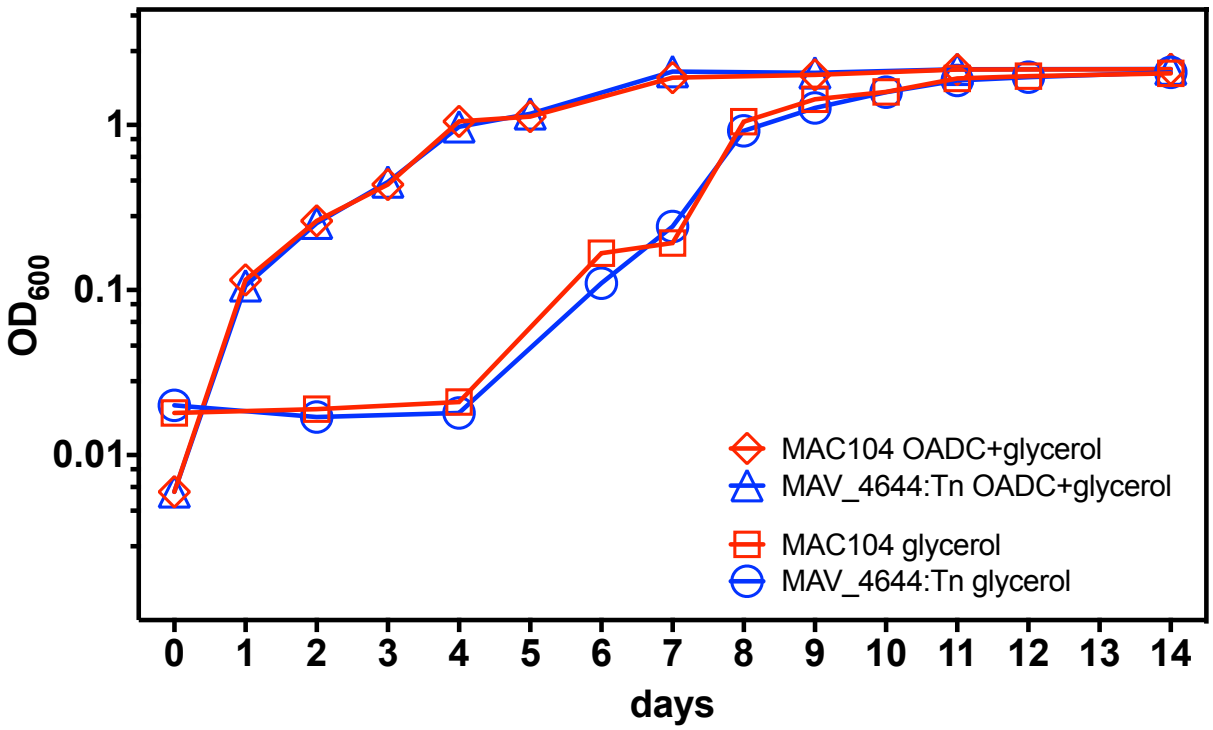

Figure 9: The growth kinetics of MAC104 and MAV_4644:Tn are similar whether assayed in 7H9 broth supplemented with 10% OADC and glycerol or 7H9 supplemented with glycerol alone. The data is representative of three separate trials.

To investigate if MAV_4644 protein is relevant in human pathogenesis, *in vitro* infection assays were performed in differentiated THP-1 human macrophage-like cells. These cells proved to be more permissive to MAH growth than RAW264.7 cells, as MAC104 displayed about a 3.5 fold increase by day 4, while MAV_4644:Tn increased by about 1.5 fold by day 4 (**figure 10).** This difference was consistently observed and MAV_4644:Tn was determined to be attenuated in the THP-1 cell line as well.

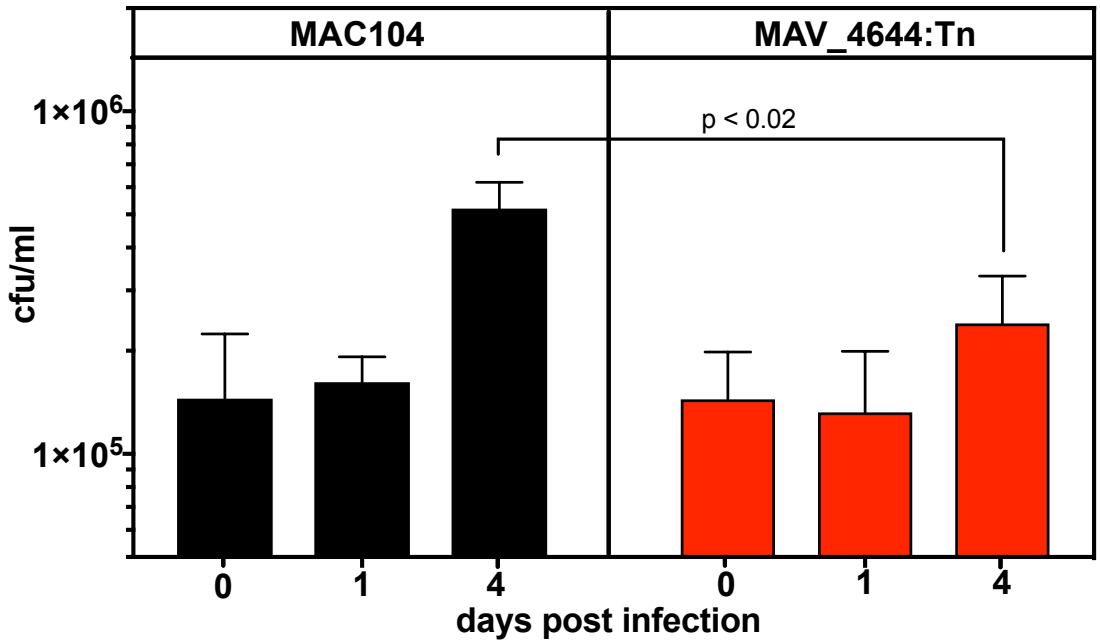

Figure 10: The human monocyte THP-1 cell line was cultured in RPMI-1640 supplemented with 10% FBS at 37°C with 5% CO_2 in 48-well plates and differentiated with 50 ng/ml of PMA for 24 hours and rested another 24 hours after media was replaced. The cells were infected separately with MAC104, MAV_4644:Tn at an MOI of 10 for 2 hours at 37°C and 5% CO_2. The cells were washed twice with HBSS and incubated for an additional 2 hours in RPMI-1640 supplemented with 10% FBS and 200ug/ml gentamicin. The cells were washed twice more with HBSS and culture media was replaced. At reported time points, the cells were lysed with 0.1% Triton X-100, serially diluted, plated on 7H10 agar and incubated at

37°C for 8-10 days before colonies were counted to assay cfu/ml. The Student's *t*-test was used to determine p-values as reported.

The invasion or uptake percentage at time 0 for MAV_4644:Tn was also consistently less than MAC104 in this cell line (data not shown) and similar to the invasion in RAW264.7 cells **(figure 5b).** In this infection model, time 0 is about 4 hours post infection due to the 2 hours of invasion and the two hours of antibiotic treatment necessary to run a long term infection. It was hypothesized that this observed difference is more likely a reflection of rapid killing by the macrophage instead of an impaired ability by MAV_4644:Tn to be phagocytosed by the host cell. To determine if this was indeed the case, short term infections were run in THP-1 cells. The mycobacteria were allowed to invade for 0.5 hours and cfu/ml were assayed up to 4 hours. At 0.5 hours post infection MAC104 and MAV_4644:Tn had been taken up at comparable levels, however by 1 hour post infection about 60% of MAV_4644:Tn had been cleared by the host cells, while the MAC104 intracellular population remained consistent throughout the duration of the experiment **(figure 11).** This data suggests the function of MAV_4644 protein serves to protect MAH from rapid killing in host macrophage and is not involved in uptake or invasion in macrophage infection.

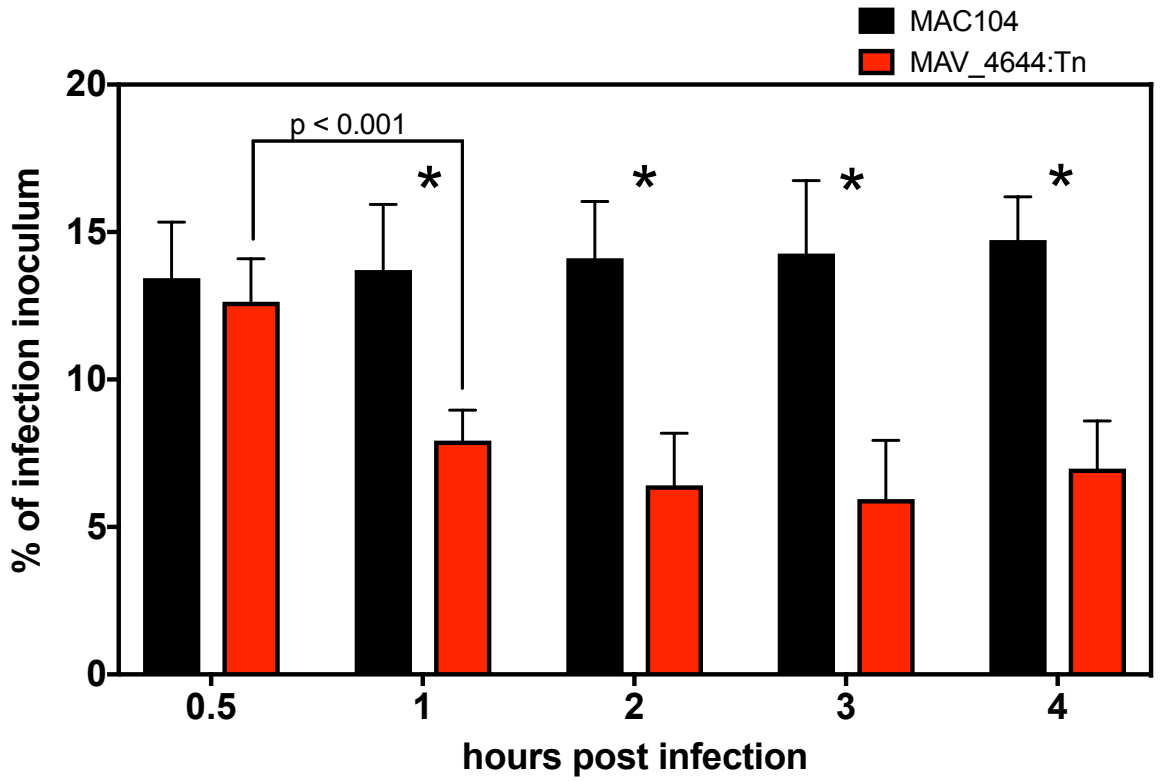

Figure 11: THP-1 macrophages were cultured in RPMI-1640 supplemented with 10% FBS at 37°C with 5% CO_2 in 48-well plates and differentiated with 50 ng/ml of PMA for 24 hours and rested another 24 hours after media was replaced. The cells were infected separately with MAC104, MAV_4644:Tn at an MOI of 10 for 30 min at 37°C and 5% CO_2. The cells were washed twice with HBSS and cells were lysed for time-0, while RPMI-1640 supplemented with 10% FBS was replaced for subsequent time points. The cells were lysed with 0.1% Triton X-100, serially diluted, plated on 7H10 agar and incubated at 37°C for 8-10 days before colonies were counted to assay cfu/ml. The Student's *t*-test was used to determine p-values as reported or * = p< 0.04.

Characterization of MAV_4644_CTD, MAV_4643, and MAV_4642 recombinant protein

The whole MAV_4644 protein was not produced (technical difficulties) rather the C-terminal region, corresponding to the VIP2 domain was expressed and denoted MAV_4644_CTD. Due to the nearly identical N-terminal regions of MAV_4644 protein and CpnT, it is hypothesized that the CTD of MAV_4644 also undergoes proteolytic cleavage before secretion or is present on the outer membrane of MAH and is capable of interacting

with host proteins (Danilchanka et al, 2014). The upstream Esat6-like secretion proteins encoded by MAV_4643 and MAV_4642 could be secreted by the pore formed by oligimerization of MAV_4644 NTD (Sun et al 2014).

To investigate potential host-protein binding partners for MAV_4644_CTD, MAV_4643, and MAV_4642 proteins, immunoprecipitation assays were performed with THP-1 cell-line clarified lysates. MAV_4644_CTD interacted with three host proteins **(table 3)**. The most noteworthy is the lysosomal peptidase cathepsin Z, which was also pulled-down by MAV_4643 and MAV_4642 proteins. MAV_4643 interacted with 6 other host proteins, including complement component 1 and cadherin 4. MAV_4642 pulled down 145 host proteins, including cathepsin S and beta-2-microglubulin **(table 3).**

The protein-protein interactions of MAV_4644_CTD were further investigated by far Western blotting. THP-1 host cell lysate was probed with MAV_4644_CTD and identified an approximately 50 kD host interacting protein. The identified protein band appears to correspond to an approximate 50 kD isoform of cathepsin Z **(figure 12).**

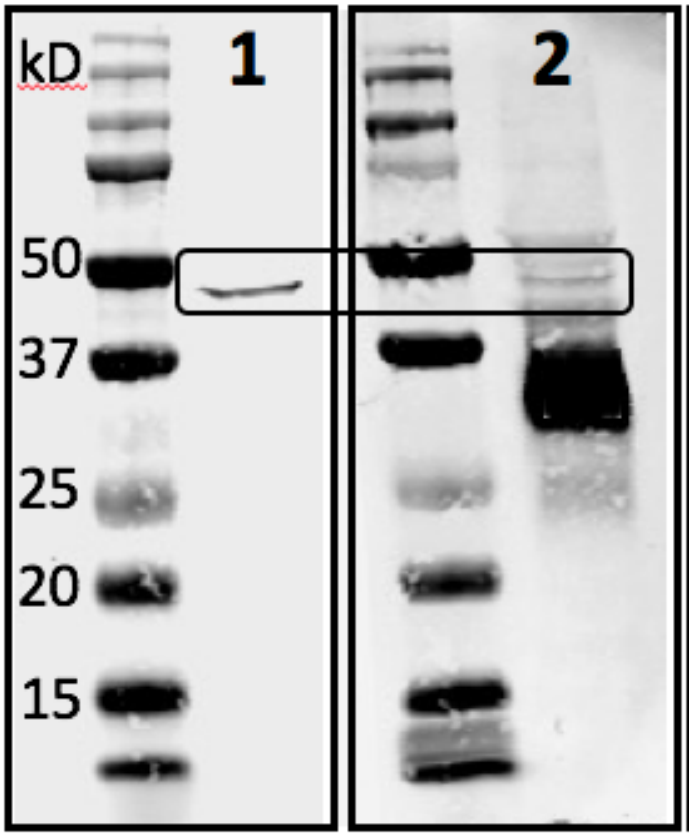

Figure 12: Far Western blot of the THP-1 host protein interaction with MAV_4644_CTD. 50 µg of cleared THP-1 cell lysate was resolved with SDS-PAGE per lane and transferred to a nitrocellulose membrane. The host proteins in lane 1 were probed with MAV_4644_CTD followed by 6xHN antibody, while the proteins in lane 2 were probed with cathepsin Z antibody. The black box identifies bands of similar mass and shape in both lanes.

Table 3: Immunoprecipitation of THP-1 protein by MAV_4644_CTD, MAV_4643, and MAV_4642 recombinant proteins. MAH proteins were produced using traditional cloning methods and captured on His-60 Ni Superflow gravity columns. Host lysate was added to the columns and incubated over night at 4°C with gentle inversion. The columns were washed and then bound proteins were eluted. The proteins were sequenced using LC-MS MS at the Oregon State University Mass Spectrometry Center.

MAV_4644_CTD protein		
Accession	**Description**	**MW [kDa]**
Q5U000	Cathepsin Z	33.8
A8K9C4	Elongation factor 1-alpha	50.2
B3KUJ0	Splicing factor 3B subunit 4	44.5
MAV_4643 protein		
Accession	**Description**	**MW [kDa]**
Q9H4X1	Regulator of cell cycle RGCC	14.6
Q5U000	Cathepsin Z	33.8
A0A0K2BMD8	Mutant hemoglobin alpha 2 globin chain	15.2
A8K651	complement component 1, q subcomponent binding protein (C1QBP)	31.4
B4E3D4	Transmembrane glycoprotein NMB	68
I3L2P9	GRB2-related adapter protein	22.1
B2RCN5	cadherin 4, type 1, R-cadherin	100.2
MAV_4642 protein		
Accession	**Description**	**MW [kDa]**
Q5U000	Cathepsin Z	33.8
A6XMH4	Beta-2-microglobulin	14.4
A0A024RBH2	Cytoskeleton-associated protein 4, isoform CRA_c	66
Q6PJ75	Integrin beta	83.6
A8K9C4	Elongation factor 1-alpha	50.2
A0A060CZ20	MHC class I antigen	53.8
P11279	Lysosome-associated membrane glycoprotein 1	44.9
A8K7Q1	nucleobindin 1 (NUCB1)	23.9
G8JLB6	Heterogeneous nuclear ribonucleoprotein H	51.2
P21757	Macrophage scavenger receptor types I and II	49.7
D3DPU2	Adenylyl cyclase-associated protein	51.6
A0A024F8H3	MHC class I antigen	40.4
A8K329	scaffold attachment factor B (SAFB)	102.7
Q86VB7	Scavenger receptor cysteine-rich type 1 protein M130	125.4
Q8N1C8	HSPA9 protein	73.8
A8K259	serpin peptidase inhibitor, clade H (heat shock protein 47), member 1	46.5
Q9BRR6	ADP-dependent glucokinase	54.1
Q59FF0	EBNA-2 co-activator variant	107.4
P25774	Cathepsin S	37.5
Q9HAT2	Sialate O-acetylesterase	58.3
B4E3D4	Transmembrane glycoprotein NMB	68
B2RE46	ribophorin II (RPN2)	69.3
A0A024R0Q4	Phospholipase D family, member 3, isoform CRA_b	54.7
A8K3K1	actin, alpha, cardiac muscle (ACTC)	42
A0A024RB16	Family with sequence similarity 62 (C2 domain containing)	123.9
J3KNL6	Protein transport protein Sec16A	251.7
F8VXC8	SWI/SNF complex subunit SMARCC2	136.1
B4DJ30	Neutral alpha-glucosidase AB	112.9
A0A024RAD5	Dolichyl-diphosphooligosaccharide--protein glycosyltransferase	50.7

Table 3 continued:

P05362	Intercellular adhesion molecule 1	57.8
Q13435	Splicing factor 3B subunit 2	100.2
Q53HV2	Chaperonin containing TCP1, subunit 7 (Eta) variant	59.3
A0A087WSV8	Nucleobindin 2, isoform CRA_b	50.2
B2R6S9	low density lipoprotein receptor-related protein associated protein 1	41.5
Q58EY4	SWI/SNF related, matrix associated, actin dependent regulator of chromatin	122.8
B2R7P8	5-aminoimidazole-4-carboxamide ribonucleotide formyltransferase	64.6
B5BUE6	ATP-dependent RNA helicase DDX5	69.1
Q5VZU9	Tripeptidyl-peptidase 2	139.7
Q9P0K7	Ankycorbin	110
B7Z6Z4	Myosin light polypeptide 6	26.7
B7Z507	Matrix metalloproteinase-9	71.5
Q9HCC0	Methylcrotonoyl-CoA carboxylase beta chain, mitochondrial	61.3
P09382	Galectin-1	14.7
Q6ICQ8	ARHG protein	21.3
Q8NCA5	Protein FAM98A	55.4
B2RDQ3	splicing factor, arginine/serine-rich 10	33.7
Q06830	Peroxiredoxin-1	22.1
A6NC86	phospholipase A2 inhibitor and Ly6/PLAUR domain-containing protein	21.9
B8XPJ8	Membrane bound catechol-O-methyltransferase	30
A0A024QZY5	PRP4 pre-mRNA processing factor 4 homolog B	116.9
J3KPS3	Fructose-bisphosphate aldolase	39.8
P39023	60S ribosomal protein L3	46.1
A0A024R5X3	SAFB-like, transcription modulator, isoform CRA_b	131.5
B7ZLW0	LPP protein	65.7
P23526	Adenosylhomocysteinase	47.7
A0A0J9YXJ0	CUGBP Elav-like family member 2	57.1
A8K517	Ribosomal protein S23, isoform CRA_a	15.8
E9PRY8	Elongation factor 1-delta	76.5
Q4LE40	C14orf159 variant protein	68
A8MUS3	60S ribosomal protein L23a	21.9
Q59H77	T-complex protein 1 subunit gamma	63.5
P26641	Elongation factor 1-gamma	50.1
E7D7X9	Pyrroline-5-carboxylate reductase	33.4
P50990	T-complex protein 1 subunit theta	59.6
F8VU51	YLP motif-containing protein 1	160.6
Q1HBJ4	Mitogen-activated protein kinase	41.4
B7Z4C8	60S ribosomal protein L31	15.1
Q8WUA2	Peptidyl-prolyl cis-trans isomerase-like 4	57.2
A8K6V3	splicing factor 3b, subunit 3, 130kDa (SF3B3)	135.5
P62701	40S ribosomal protein S4, X isoform	29.6
P23219	Prostaglandin G/H synthase 1	68.6
A0A0S2Z5U3	Heterogeneous nuclear ribonucleoprotein L-like isoform 2	63.6
Q96ST3	Paired amphipathic helix protein Sin3a	145.1
B2R4C0	60S ribosomal protein L18a	20.7
P62633	Cellular nucleic acid-binding protein	19.4
Q7L2J0	7SK snRNA methylphosphate capping enzyme	74.3
B4DNE1	Basigin	42.2
G3V2S9	SRA stem-loop-interacting RNA-binding protein, mitochondrial	13.9
Q13595	Transformer-2 protein homolog alpha	32.7
A0A0A6YYJ8	Putative RNA-binding protein Luc7-like 2	54.2
Q9Y4E8	Ubiquitin carboxyl-terminal hydrolase 15	112.3
P11215	Integrin alpha-M	51

Table 3 continued:

Q8IVS2	Malonyl-CoA-acyl carrier protein transacylase, mitochondrial	42.9
Q9NYF8	Bcl-2-associated transcription factor 1	37.5
A0A0D9SGE8	PHD finger protein 6	41.3
Q9H0N5	Pterin-4-alpha-carbinolamine dehydratase 2	14.4
P23368	NAD-dependent malic enzyme, mitochondrial	22.8
Q6U8A4	Ubiquitin-specific protease 7 isoform	128.9
O43290	U4/U6.U5 tri-snRNP-associated protein 1	90.2
A0A0S2Z570	Retinoid X receptor beta isoform 2	57.3
A0A024R845	RAB14, member RAS oncogene family, isoform CRA_a	40.9
A0A024R5Q4	Glycine amidinotransferase (L-arginine:glycine amidinotransferase)	54.1
Q53Z07	NPC-A-16	21.8
O15294	UDP-N-acetylglucosamine--peptide N-acetylglucosaminyltransferase	116.8
A0A0C4DG17	40S ribosomal protein SA	33.3
B4DJQ5	Glucosidase 2 subunit beta	60.1
P54886	Delta-1-pyrroline-5-carboxylate synthase	87.2
Q53FI7	Four and a half LIM domains 1 variant (Fragment)	31.9
O14874	[3-methyl-2-oxobutanoate dehydrogenase [lipoamide]] kinase	46.3
A0A090KM56	HLA class I antigen	40.3
B2R6P1	galactosamine (N-acetyl)-6-sulfate sulfatase	57.9
Q8TD55	Pleckstrin homology domain-containing family O member 2	53.3
P62979	Ubiquitin-40S ribosomal protein S27a	18
A0A0A0MT83	Isovaleryl-CoA dehydrogenase, mitochondrial	46.6
A0A024QZN9	Voltage-dependent anion channel 2, isoform CRA_a	34.5
E7EMB3	Calmodulin	21.7
Q9BWJ5	Splicing factor 3B subunit 5	10.1
Q59GK9	Ribosomal protein L21 variant (Fragment)	18.9
A0A024R608	Ribosomal protein, large, P1, isoform CRA_a	11.5
Q9NW64	Pre-mRNA-splicing factor RBM22	46.9
P20674	Cytochrome c oxidase subunit 5A, mitochondrial	16.8
O43660	Pleiotropic regulator 1	57.2
Q9C0J8	pre-mRNA 3' end processing protein WDR33	145.8
Q9BV19	Uncharacterized protein C1orf50	21.9
Q05DF2	SF3A2 protein	51.4
Q9Y2W1	Thyroid hormone receptor-associated protein 3	108.6
P52948	Nuclear pore complex protein Nup98-Nup96	197.5
A0A0U1RRM4	Polypyrimidine tract-binding protein 1	62.4
B4E141	golgi SNAP receptor complex member 2	26.9
Q13405	39S ribosomal protein L49, mitochondrial	19.2
Q14241	Transcription elongation factor B polypeptide 3	89.9
Q9Y6M5	Zinc transporter 1	55.3
Q59EI9	ADP,ATP carrier protein, liver isoform T2 variant	35.4
Q9Y2X9	Zinc finger protein 281	96.9
Q13151	Heterogeneous nuclear ribonucleoprotein A0	30.8
B2R9K8	chaperonin containing TCP1, subunit 6A (zeta 1)(CCT6A)	57.9
P14317	Hematopoietic lineage cell-specific protein	54
B4DIV8	Tripeptidyl-peptidase 1 (EC 3.4.14.9)	62.2
J3QK89	Calcium homeostasis endoplasmic reticulum protein	104.9
Q16629	Serine/arginine-rich splicing factor 7	27.4
Q6PJT7	Zinc finger CCCH domain-containing protein 14	82.8
Q6IPI1	Ribosomal protein L29	17.9
A0A024RDE8	PDZ and LIM domain 5, isoform CRA_c	63.9
Q15717	ELAV-like protein 1	36.1
P56270	Myc-associated zinc finger protein	48.6

Knock-down of cathepsin Z protein in THP-1 cells and subsequent MAH infections

Cathepsin Z was knocked-down in THP-1 cells using Dicer-substrate short interfering RNAs. At 4 days-post transfection, the cathepsin Z protein concentration was significantly diminished compared to the negative controls **(figure 12a.).** A one-hour survival assay was then performed. In cathepsin Z knocked-down cells, MAV_4644:Tn survived near wild-type levels and was significantly more virulent than in the negative controls **(figure 12b.)** MAC104 survived similarly in both knock-down conditions, though less than in untreated cells. This data suggest cathepsin Z is involved in early mycobacterial killing within host macrophages and MAV-4644 protein is involved in suppressing this function.

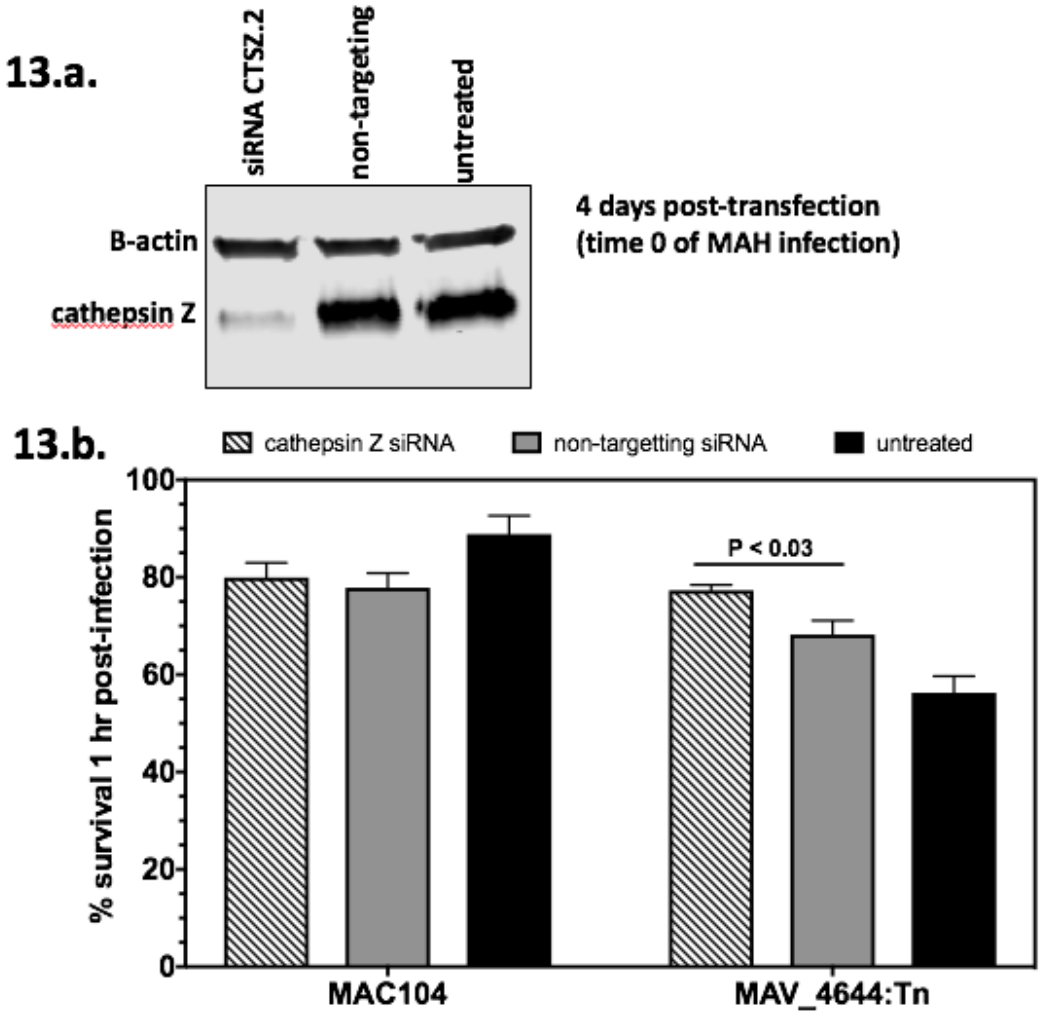

Figure 13: (a) Western-blot of cathepsin Z protein concentrations of transfected THP-1 macrophages at 4 days post-transfection and time 0 of infection. **(b)** One-hour survival assay of MAC104 and MAV_4644:Tn within cathepsin z knocked-down THP-1 macrophages and negative controls. Data is reported as the average and standard error of two separate experiments. The Student's *t*-test was used to determine p-values as reported.

CHAPTER 1. Discussion

MAH replicates within IFN-γ stimulated macrophages that produce nitric oxide

The mycobacterial response to nitric oxide within the host macrophage plays an important role in the survival and replication of these intracellular pathogens. MAH displays increased virulence during infections in wild-type mice when compared to NOS2 knock-out mice (Gomes 1999). This observation was validated in this study in an *in vitro* model. We show that murine macrophages stimulated with IFN-γ and producing nitric oxide are permissive to intracellular growth of MAH and that intracellular growth was abrogated if the macrophages were treated with an inhibitor of nitric oxide production or if IFN-γ was withheld. In this model the macrophages untreated with IFN-γ and infected with MAH were capable of robust production of nitric oxide near the levels of IFN-γ activated cells. Nevertheless, these cells were not permissive to MAH growth indicating a multifunctional role of nitric oxide during infection with MAH. Indeed, nitric oxide has multiple and converse roles within macrophages and is a potent cellular effector of immune signaling (Bogdan 2001, Lowenstein 2004). Depending on the concentration, nitric oxide can trigger or suppress apoptosis in inflammatory macrophages (Taylor 2003). In addition, nitric oxide has been shown to protect cells from LPS induced shock by acting as a negative regulator of the NLRP3 inflammasome, a key intracellular trigger of inflammation (Mao 2013).

The observation that most of the MAH MmT7 nitric oxide susceptible mutants grew to wild-type levels within macrophages could suggests that the nitric oxide levels in the susceptibility assay were greater than those in the phagosome. Other studies have also shown that nitric oxide susceptibility does not correlate with the virulence of *M. avium*

strains in murine infection (Lousada 2007, Ehlers 1999, Lousada 2006). Another possibility could be that MAH becomes more resistant to nitric oxide after phagocytosis. This could be explained by contact with the host cell triggering a shift in the mycobacterial phenotype towards pathogenesis. MAH are capable of such a shift, as it has been shown that passage of MAH through macrophages improves its ability to infect subsequent macrophages (Bermudez 1997, Early 2011). Furthermore, it is well documented that MTB employs a dramatic transcriptional response, which is required for virulence, upon encountering the host cell and MAH most likely does as well (Green 2014, Spiro 2007, Voskuil 2003).

It is well established that MAH infection is not hindered by the presence of nitric oxide, but the task of understanding how nitric oxide adds to the success of MAH is more difficult. It has been put forth that many bacterial pathogens, such as *P. aeruginosa, E. coli, S. aureus,* and *S. typhimurium*, express nitrate, nitrite and nitric oxide reductases as virulence factors to metabolize these products into energy and to detoxify their respective intracellular niches (Vazquez-Torres 2015). Similar observations have been made with pathogenic mycobacteria, positing that the organisms are capable of nitrogen metabolism as an energy source and correlate with a positive effect on bacterial survival (Tan 2010). For example, the nitrate reductase gene, *narG*, was required by MTB for intracellular growth (Sohaskey 2008). Also, an MAH mutant in the gene MAV_4012, which encodes a hypothetical protein directly downstream of a nitric oxide reductase subunit, displayed attenuated virulence in a murine model of infection (Li 2009).

Nitric oxide serves as a potent signaling molecule and bactericidal effector within host macrophages. Regardless, MAH survives and replicates under nitrosative stress. It

could be that the nitric oxide signal shapes the macrophage to a more permissive state or that it serves as a virulence activator for the bacterium or as a terminal electron acceptor in anaerobic metabolism. Furthering the understanding of this relationship could lead to new therapeutic options for treating infections with pathogenic mycobacteria.

Characterization of MAV_4644

MAV_4644 is a putative ADP-ribosyltransferase (ADPRT), which is highly conserved throughout pathogenic mycobacteria and homologous to the dual function channel protein with necrosis inducing toxin, Cpnt (Rv3903c) of MTB. The homologous N-terminal domains (NTD) are highly conserved in their primary sequences and the NTD of Cpnt has been shown to be a channel protein required for uptake of glycerol (Danilchanka 2013, Sun 2015). MAV_4644:Tn displayed similar growth kinetics to wild-type MAH in media with glycerol as the sole carbon source, which could indicate a different function for this protein in MAH. However, a search for paralogous genes to MAV_4644 in the genome of MAC104 revealed MAV_2415, which could also be a channel protein for glycerol uptake. There are no paralogous genes to Rv3903c in the genome of H37Rv. These findings could explain the differing phenotypes in the face of obvious identity. Interestingly, MAV_2415 does not share operonic conservation with MAV_4644 or Rv3903c.

The CTD of Cpnt is a secreted necrotizing toxin with glycohydrolase activity and differs greatly from the CTD of MAV_4644, which is an ADPRT of the VIP2 super family. This family consists of toxins of pathogenic bacteria such as, *Pseudomonas aeruginosa* exoenzyme S (ExoS), *Vibrio cholerae* cholera toxin, *Bordetella pertussis* pertussis toxin, and

Corynebacterium diphtheriae diphtheria toxin. In general, these proteins transfer ADP-ribose from NAD to host proteins, halting key cellular processes and intoxicating the host cell. (Castagnini 2012). A pairwise alignment analysis in pBLAST of the primary protein sequences between the VIP2 domains of MAV_4644 and other known toxins revealed considerable conservation between MAV_4644 and ExoS of *P. aeruginosa,* as they aligned over 92% of the domain with an E-value of 2.00E-16.

ExoS is a type III secretion effector with a GTPase activating domain and an ADPRT domain, which is required for virulence in *P. aeruginosa* (Rocha 2003, Knight 2005). ExoS ADP-ribosylates Rab4, affecting its role in membrane trafficking, and greatly inhibits transferrin recycling (Betta-Bobillo 1998). ExoS also intoxicates cells by ribosylating Rab5 with ADP and interrupting endosome fusion (Barbieri 2000). It has also been shown that the ADPRT activity of ExoS is required for *P. aeruginosa* to disrupt the pulmonary-vascular barrier during pneumonic infection and to disseminate into the blood (Rangel 2015). In addition, a robust *in silico* analysis of structural motifs and sequence identity was used to build computational models towards the identification of novel ADPRT toxins in bacterial pathogens and MAV_4644 of MAH was indeed identified as an ExoS-like toxin (Fieldhouse 2010). Interestingly, there is evidence for this family of toxins, being spread by horizontal gene transfer between bacterial species, as well as across kingdoms (Pallen 2001). Many ADPRT genes are encoded by mobile genetic elements, such as bacteriophages, pathogenicity islands and plasmids, enabling promiscuity of this gene family (Glowacki 2002). In fact, the ADPRT domain of MAV_4644 is 53% GC, while the rest of the gene is 74%, which could be explained by horizontal gene transfer.

MAV_4644 is in an operon with MAV_4643 and MAV_4642, which are Esat-6 and CFP-10-like, and homologs of MTB esxE and esxF, respectively. Esat-6 and CFP-10 are a pair of sequential effector proteins secreted by the ESX-1 type VII secretion system of MTB and are required for virulence (Simeone 2015, Ohol 2010, Sreejit 2014, Renshaw 2002). All other Esat-6 and CFP-10 like gene pairs of both MAH and MTB are associated in a gene cluster with ESX type VII secretion systems (Bitter 2009). The fact that MAV_4643, MAV_4642 and their homologs esxE and esxF are upstream of a channel forming protein adds considerable weight to the potential of MAV_4644 operon also being a secretion system of mycobacteria.

MAV_4644:Tn is attenuated in macrophages and displayed a rapid decline in the intracellular population in the first hour following macrophage infection. The function of MAV_4644 protein and/or operonic partners appears to protect the bacteria from early macrophage killing. This role could be served by secreting the operonic proteins or other virulence effectors through the putative pore. MAV_4644_CTD interacts with host protein cathepsin Z in an immunoprecipitation assay and a 50 kD host protein in a far Western, which could possibly be a heavier isoform or post translationally modified cathepsin Z. MAV_4643 and MAV_4642 recombinant proteins also interacted with cathepsin Z. This could indicate that the proteins of the operon work together in complex to interact with the host protein.

Cathepsins are lysosomal peptidases and important regulators of inflammation and cell death within macrophages (Conus 2008). There are 11 human cysteine cathepsins and many are involved in pathogenic mycobacterial infections. (Turk 2012, Pires 2016).

Infection with MAH and MTB inhibit the maturation of cathepsin L, while infection with *M. bovis* BCG inhibits expression of cathepsin S (Nepal 2006, Sendide 2017). Most importantly, independent studies have associated single nucleotide polymorphisms in *CTSZ* with increased susceptibility to tuberculosis (Adams 2011, Baker 2011).

Cathepsin Z is a lysosomal cysteine peptidase (Santamaria 1998). It has been positively identified as a protein of the early endosome and such proteins are accessible to the mycobacterial vacuole (Garin 2001, Sturgill-Koszycki 1996). Cathepsin Z has also been reported to be critical for degrading polyglutamine-containing proteins within lysosomes. The cell membranes of pathogenic mycobacteria have numerous polyglutamine stretches (Bhutani 2012, Tripathi 2003, Garg 2015). Cathepsin Z could act on the mycobacterial membrane early in infection, killing a subset of the phagocytosed bacterium. The secreted gene products of the MAV_4644 operon could serve to protect MAH from the peptidase, explaining the attenuation of the mutant. MAV_4644 could ADP-ribosylate and inactivate cathepsin Z or MAV_4643 protein and MAV_4642 protein could interact with the active site or induce allosteric changes through protein-protein interactions **(figure 14).**

To investigate this hypothesis, cathepsin Z protein was knocked-down in macrophages and subsequent infection with MAV_4644:Tn and MAC104 followed. The knock-down of cathepsin Z in host macrophages rescued the attenuated phenotype of MAV_4644:Tn to near wild-type levels of survival. The data suggests cathepsin Z is involved in early mycobacterial killing within host macrophages and virulence factor MAV_4644 protein abrogates this process.

This work adds to the understanding of the MAH response to nitric oxide within macrophages and identified MAV_4644 as a virulence factor for MAH. In addition, the lysosomal peptidase cathepsin Z is shown to be involved in early macrophage killing of mycobacteria. Future studies into this process could identify potential new therapeutic agents against MAH and further the knowledge of macrophage killing methods.

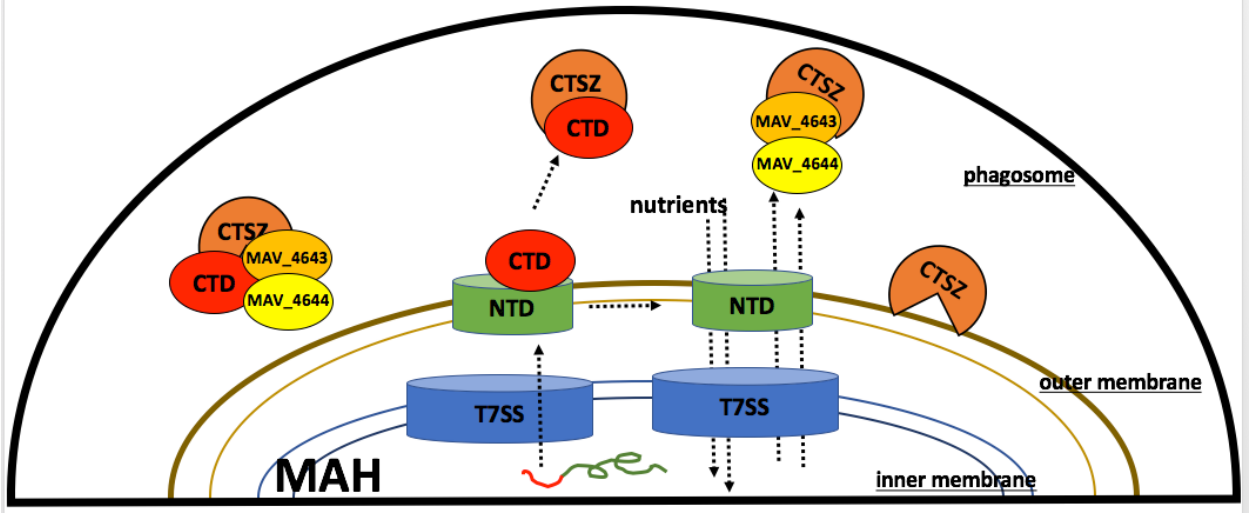

Figure 14: Hypothetical model of MAV_4644 protein interaction with cathepsin z in macrophage phagosome. MAV_4644 protein is transported via T7SS and assembles on the outer membrane. CTD is secreted through proteolytic cleavage, allowing CTD to interact with CTSZ, and opening NTD to transport nutrients and proteins. **T7SS**: type 7 secretion system, **NTD**: MAV_4644 protein N-terminal domain, **CT**D: MAV_4644 protein C-terminal domain, **CTSZ**: cathepsin Z protein

CHAPTER 1. References

Al Houqani, M., Jamieson, F., Chedore, P., Mehta, M., May, K., & Marras, T. K. (2011). Isolation prevalence of pulmonary nontuberculous mycobacteria in Ontario in 2007. *Canadian Respiratory Journal*, *18*(1), 19–24.

Amer, A. O., & Swanson, M. S. (2002). A phagosome of one ' s own: a microbial guide to life in the macrophage. *Curr Opin Microbiol.*, *5*(1), 56–61.

Andrés Vazquez-Torres*, Tania Stevanin†, Jessica Jones-Carson*, Margaret Castor‡, Robert C. Read†, and F. C. F. (2008). Analysis of Nitric Oxide-Dependent Antimicrobial Actions in Macrophages and Mice. *Methods Enzymol*, *437*, 521–538.

Barbieri, A. M., Sha, Q., Bette-Bobillo, P., Stahl, P. D., & Vidal, M. (2001). ADP-ribosylation of Rab5 by ExoS of Pseudomonas aeruginosa affects endocytosis. *Infection and Immunity*, *69*(9), 5329–5334.

Beisiegel, M., Kursar, M., Koch, M., Loddenkemper, C., Kuhlmann, S., Zedler, U., … Kaufmann, S. H. E. (2009). Combination of Host Susceptibility and Virulence of *Mycobacterium tuberculosis* Determines Dual Role of Nitric Oxide in the Protection and Control of Inflammation. *The Journal of Infectious Diseases*, *199*(8), 1222–1232.

Bermudez, L. E., & Parker, A. M. Y. (1997). Growth within macrophages increases the efficiency of Mycobacterium avium in invading other macrophages by a complement receptor-independent pathway . Infect. Immun. 65:1916–1925.

Bette-Bobillo, P., Giro, P., Sainte-Marie, J., & Vidal, M. (1998). Exoenzyme S from P. aeruginosa ADP ribosylates rab4 and inhibits transferrin recycling in SLO-permeabilized reticulocytes. *Biochemical and Biophysical Research Communications*, *244*(2), 336–41.

Bhutani, N., Piccirillo, R., Hourez, R., Venkatraman, P., & Goldberg, A. L. (2012). Cathepsins L and Z are critical in degrading polyglutamine-containing proteins within lysosomes. *Journal of Biological Chemistry*, *287*(21), 17471–17482.

Bitter, W., Houben, E. N. G., Bottai, D., Brodin, P., Brown, E. J., Cox, J. S., … Brosch, R. (2009). Systematic genetic nomenclature for type VII secretion systems. *PLoS Pathogens*, *5*(10), 8–13.

Bogdan, C. (2001). Nitric oxide and the immune response. *Nature Immunology*, *2*(10), 907–16

Bogdan, C. (2015). Nitric oxide synthase in innate and adaptive immunity: An update. *Trends in Immunology*, *36*(3), 161–178.

Briken, V., Ahlbrand, S. E., & Shah, S. (2013). Mycobacterium tuberculosis and the host cell inflammasome: a complex relationship. *Frontiers in Cellular and Infection Microbiology*, *3*(October), 62.

Cook, G., Berney, M., & Gebhard, S. (2009). Physiology of mycobacteria. *… in Microbial Physiology*, *2911*(9).

Conus, S., & Simon, H. U. (2008). Cathepsins: Key modulators of cell death and inflammatory responses. *Biochemical Pharmacology*, *76*(11), 1374–1382.

Cosma, C. L., Sherman, D. R., & Ramakrishnan, L. (2003). The secret lives of the pathogenic mycobacteria. *Annual Review of Microbiology*, *57*(1), 641–676.

Doi, T., Ando, M., Akaike, T., Suga, M., Sato, K., & Maeda, H. (1993). Resistance to nitric oxide in Mycobacterium avium complex and its implication in pathogenesis. *Infection and Immunity*, *61*(5), 1980–1989.

Early, J., Fischer, K., & Bermudez, L. E. (2011). Mycobacterium avium uses apoptotic macrophages as tools for spreading. *Microbial Pathogenesis*, *50*(2), 132–139.

Egelund, E.F., Fennelly K.P., Peloquin C.A. (2015). Medications and monitoring in nontuberculous mycobacteria infections. *Clinics in Chest Medicine,36*(1), 55-66.

Escuyer, V., Haddad, N., Frehel, C., & Berche, P. (1996). Molecular characterization of a surface-exposed superoxide dismutase of Mycobacterium avium. *Microbial Pathogenesis*, *20*(1), 41–55.

Ferric C. Fang. (2004). Antimicrobial reactive oxygen and nitrogen species: concepts and controversies. *Nature Reviews Microbiology*, *2*(10), 820–832.

Field, S. K., Fisher, D., & Cowie, R. L. (2004). Mycobacterium avium complex pulmonary disease in patients without HIV infection. *Chest*, *126*(2), 566–81.

Garin, J., Diez, R., Kieffer, S., Dermine, J. F., Duclos, S., Gagnon, E., … Desjardins, M. (2001). The phagosome proteome: Insight into phagosome functions. *Journal of Cell Biology*, *152*(1), 165–180.

Glowacki, G., Braren, R., Firner, K., Nissen, M., Reche, P., Bazan, F., … Koch-nolte, F. (2002). The family of toxin-related ecto-ADP- ribosyltransferases in humans and the mouse. *Protein Science*, *11*, 1657–1670.

Gomes, M. S., Flórido, M., Pais, T. F., & Appelberg, R. (1999). Improved clearance of Mycobacterium avium upon disruption of the inducible nitric oxide synthase gene. *Journal of Immunology (Baltimore, Md. : 1950)*, *162*(11), 6734–6739.

Gomez-Smith, C. K., Lapara, T. M., & Hozalski, R. M. (2015). Sulfate reducing bacteria and mycobacteria dominate the biofilm communities in a chloraminated drinking water distribution system. *Environmental Science and Technology*, *49*(14), 8432–8440.

Green, J., Rolfe, M. D., & Smith, L. J. (2014). Transcriptional regulation of bacterial virulence gene expression by molecular oxygen and nitric oxide. *Virulence*, *5*(4), 1–16.

Inderlied, C. B., Kemper, C. A., & Bermudez, L. E. M. (1993). The Mycobacterium avium Complex, *6*(3), 266–310.

Ishikane, M., & Tanuma, J. (2014). Mycobacterium avium complex enteritis in HIV-infected patient. *IDCases*, *1*(2), 22–23.

Jung, J. Y., Madan-Lala, R., Georgieva, M., Rengarajan, J., Sohaskey, C. D., Bange, F. C., & Robinson, C. M. (2013). The intracellular environment of human macrophages that produce nitric oxide promotes growth of mycobacteria. *Infection and Immunity*, *81*(9), 3198–3209.

Kelley, V. A., Schorey, J. S., Dame, N., & Dame, N. (2003). Mycobacterium ' s Arrest of Phagosome Maturation in Macrophages Requires Rab5 Activity and Accessibility to Iron, *14*(August), 3366–3377.

Knight, D. A., Kulich, S. M., Barbieri, J. T., Knight, D. A., Finck-barbanc, V., Kulich, S. M., & Barbieri, J. T. (1995). Functional Domains of Pseudomonas aeruginosa Exoenzyme S, *63*(8), 3182–3186.

Lai, C. C., Tan, C. K., Chou, C. H., Hsu, H. L., Liao, C. H., Huang, Y. T., … Hsueh, P. R. (2010). Increasing incidence of nontuberculous mycobacteria, Taiwan, 2000-2008. *Emerging Infectious Diseases*, *16*(2), 294–296

Lousada, S., Flórido, M., & Appelberg, R. (2007). Virulence of Mycobacterium avium in mice does not correlate with resistance to nitric oxide. *Microbial Pathogenesis*, *43*(5–6), 243–248.

Lousada, S., Flórido, M., & Appelberg, R. (2006). Regulation of granuloma fibrosis by nitric oxide during Mycobacterium avium experimental infection. *International Journal of Experimental Pathology*, *87*(4), 307–315.

Mao, K., Chen, S., Chen, M., Ma, Y., Wang, Y., Huang, B., … Sun, B. (2013). Nitric oxide suppresses NLRP3 inflammasome activation and protects against LPS-induced septic shock. *Cell Research*, *23*(2), 201–12.

Marrakchi, H., Laneelle, M. A., & Daffe, M. (2014). Mycolic acids: Structures, biosynthesis, and beyond. *Chemistry and Biology*, *21*(1), 67–85.

McNamara, M., Tzeng, S.-C., Maier, C., Wu, M., & Bermudez, L. E. (2013). Surface-exposed proteins of pathogenic mycobacteria and the role of Cu-Zn superoxide dismutase in macrophages and neutrophil survival. *Proteome Science*, *11*(1), 45.

Nepal, R. M., Mampe, S., Shaffer, B., Erickson, A. H., & Bryant, P. (2006). Cathepsin L maturation and activity is impaired in macrophages harboring M. avium and M. tuberculosis. *International Immunology*, *18*(6), 931–939.

Orme, I. M., & Ordway, D. J. (2014). Host response to nontuberculous mycobacterial infections of current clinical importance. *Infection and Immunity*, *82*(9), 3516–3522.

Pallen, M. J., Lam, A. C., Loman, N. J., & McBride, A. (2001). An abundance of bacterial ADP-ribosyltransferases - Implications for the origin of exotoxins and their human homologues. *Trends in Microbiology*, *9*(7), 302–308

Papadopoulos, J. S., & Agarwala, R. (2007). COBALT: Constraint-based alignment tool for multiple protein sequences. *Bioinformatics*, *23*(9), 1073–1079.

Park, J.-B. (2003). Phagocytosis induces superoxide formation and apoptosis in macrophages. *Experimental & Molecular Medicine*, *35*(5), 325–335.

Pires, D., Marques, J., Pombo, J. P., Carmo, N., Bettencourt, P., Neyrolles, O., … Anes, E. (2016). Role of Cathepsins in Mycobacterium tuberculosis Survival in Human Macrophages. *Scientific Reports*, *6*(August), 32247. https://doi.org/10.1038/srep32247

Pearl, J. E., Torrado, E., Tighe, M., Fountain, J. J., Solache, A., Strutt, T., … Cooper, A. M. (2012). Nitric oxide inhibits the accumulation of CD4+CD44hiTbet+CD69lo T cells in mycobacterial infection. *European Journal of Immunology*, *42*(12), 3267–3279.

Renshaw, P. S., Panagiotidou, P., Whelan, A., Gordon, S. V., Glyn Hewinson, R., Williamson, R. A., & Carr, M. D. (2002). Conclusive evidence that the major T-cell antigens of the Mycobacterium tuberculosis complex ESAT-6 and CFP-10 form a tight, 1:1 complex and characterization of the structural properties of ESAT-6, CFP-10, and the ESAT-6:CFP-10 complex. *Journal of Biological Chemistry*, *277*(24), 21598–21603.

Rocco, J. M., & Irani, V. R. (2011). Mycobacterium avium and modulation of the host macrophage immune mechanisms. *The International Journal of Tuberculosis and Lung*

Disease : The Official Journal of the International Union against Tuberculosis and Lung Disease, *15*(4), 447–52

Rose, S. J., & Bermudez, L. E. (2016). Identification of Bicarbonate as a Trigger and Genes Involved with Extracellular DNA Export in Mycobacterial Biofilms. *mBio*, *7*(6), e01597-16. https://doi.org/10.1128/mBio.01597-16

Santamaria, I, Velasco G, Pendas AM, Fueyo A, Lopez-Otin C. Cathepsin Z, a novel human cysteine proteinase with a short propeptide domain and a unique chromosomal location. J Biol Chem 1998;273:16816–23

Sendide, K., Deghmane, A.-E., Pechkovsky, D., Av-Gay, Y., Talal, A., & Hmama, Z. (2005). Mycobacterium bovis BCG attenuates surface expression of mature class II molecules through IL-10-dependent inhibition of cathepsin S. *Journal of Immunology (Baltimore, Md. : 1950)*, *175*(8), 5324–5332.

Shiloh, M. U., MacMicking, J. D., Nicholson, S., Brause, J. E., Potter, S., Marino, M., Nathan, C. (1999). Phenotype of mice and macrophages deficient in both phagocyte oxidase and inducible nitric oxide synthase. *Immunity*, *10*(1), 29–38.

Simeone, R., Bottai, D., Frigui, W., Majlessi, L., & Brosch, R. (2015). ESX/type VII secretion systems of mycobacteria: Insights into evolution, pathogenicity and protection. *Tuberculosis (Edinburgh, Scotland)*, *95 Suppl 1*, S150-4.

Sohaskey, C. D. (2008). Nitrate enhances the survival of Mycobacterium tuberculosis during inhibition of respiration. *Journal of Bacteriology*, *190*(8), 2981–2986.

Sreejit, G., Ahmed, A., Parveen, N., Jha, V., Valluri, V. L., Ghosh, S., & Mukhopadhyay, S. (2014). The ESAT-6 Protein of *Mycobacterium tuberculosis* Interacts with Beta-2-Microglobulin (B2M) Affecting Antigen Presentation Function of Macrophage. *PLoS Pathogens*, *10*(10).

Stephen Spiro. (2007). Regulators of bacterial responses to nitric oxide. *FEMS Microbiology Reviews*, *31*(2), 193–211

Sturgill-Koszycki, S., Schaible, U. E., & Russell, D. G. (1996). Mycobacterium-containing phagosomes are accessible to early endosomes and reflect a transitional state in normal phagosome biogenesis. *The EMBO Journal*, *15*(24), 6960–8. Retrieved from

Tan, M. P., Sequeira, P., Lin, W. W., Phong, W. Y., Cliff, P., Ng, S. H., … Alonso, S. (2010). Nitrate respiration protects hypoxic Mycobacterium tuberculosisagainst acid- and reactive nitrogen species stresses. *PLoS ONE*, *5*(10), 1–8.

Tripathi, D., Chandra, H., Bhatnagar, R., Johnson, R., Streicher, E., Louw, G., … Chapman, M. (2013). Poly-L-glutamate/glutamine synthesis in the cell wall of Mycobacterium bovis is regulated in response to nitrogen availability. *BMC Microbiology*, *13*(1), 226.

Turk, V., Stoka, V., Vasiljeva, O., Renko, M., Sun, T., Turk, B., & Turk, D. (2012). Cysteine cathepsins: From structure, function and regulation to new frontiers. *Biochimica et Biophysica Acta - Proteins and Proteomics*, *1824*(1), 68–88.

Voskuil, M. I., Schnappinger, D., Visconti, K. C., Harrell, M. I., Dolganov, G. M., Sherman, D. R., & Schoolnik, G. K. (2003). Inhibition of respiration by nitric oxide induces a Mycobacterium tuberculosis dormancy program. *The Journal of Experimental Medicine*, *198*(5), 705–713.